Periodic Fast Radio Bursts from ULX-Like Binaries

Navin Sridhar ID,[1,2] Brian D. Metzger,[3,2] Paz Beniamini ID,[4,5] Ben Margalit,[6,*] Mathieu Renzo ID,[2,3] and Lorenzo Sironi[1,2]

[1]Department of Astronomy, Columbia University, New York, NY 10027, USA
[2]Columbia Astrophysics Laboratory, Columbia University, New York, NY 10027, USA
[3]Center for Computational Astrophysics, Flatiron Institute, 162 W. 5th Avenue, New York, NY 10011, USA
[4]Division of Physics, Mathematics and Astronomy, California Institute of Technology, Pasadena, CA 91125, USA
[5]Astrophysics Research Center of the Open University (ARCO), The Open University of Israel, P.O Box 808, Ra'anana 43537, Israel
[6]Astronomy Department and Theoretical Astrophysics Center, University of California, Berkeley, Berkeley, CA 94720, USA

ABSTRACT

The discovery of periodicity in the arrival times of the fast radio bursts (FRB) from two of the best studied repeating sources poses a potential challenge to oft studied magnetar scenarios. However, models which postulate that FRB emission results from relativistic magnetized shocks, or magnetic reconnection in a striped outflow, are not necessarily specific to magnetar engines, instead requiring only the impulsive injection of relativistic energy into a dense magnetized medium. Motivated thus, we outline a new scenario in which FRBs are powered by short-lived relativistic outflows ("flares") from accreting black hole or neutron star systems, which propagate into the cavity of the pre-existing ("quiescent") jet. In order to reproduce FRB luminosities and rates, we are driven to consider binaries of stellar-mass compact objects undergoing super-Eddington mass transfer, similar to those which characterize some ultra-luminous X-ray (ULX) sources. Indeed, the host galaxies of FRBs, and their spatial offsets within their hosts, show broad some similarities to those of ULX; the ULX hosts exhibit systematically lower metallicities than those of FRBs, though the comparison is complicated by different selection effects and contaminants affecting the two populations. Periodicity on timescales of days to years could be attributed to precession (e.g., Lens-Thirring) of the polar accretion funnel, along which the FRB emission is geometrically and relativistically beamed, across the observer line of sight. Accounting for the most luminous FRBs via accretion power may require a population of binaries undergoing brief-lived phases of unstable (dynamical timescale) mass transfer. This could lead to secular evolution in the burst properties of some repeating FRB sources on timescales as short as months to years, followed by a transient optical/IR counterpart akin to a luminous red nova or dusty common envelope transient. We encourage targeted FRB searches of known ULX sources.

Keywords:

1. INTRODUCTION

Fast Radio Bursts (FRB) are short, luminous pulses of coherent radio emission of extragalactic origin (Lorimer et al. 2007; Keane et al. 2012; Thornton et al. 2013). Among the many proposed models for FRBs (Platts et al. 2019), the best-studied are those which postulate flaring magnetars as their central engines (e.g., Popov & Postnov 2013; Lyubarsky 2014; Kulkarni et al. 2014;

Katz 2016; Metzger et al. 2017; Beloborodov 2017; Kumar et al. 2017; Metzger et al. 2019; Wadiasingh & Timokhin 2019). Magnetar models can account in a natural way for many of the observed properties of FRBs, including their short (≲ millisecond) timescales, large energetics, potentially high polarization (e.g., Michilli et al. 2018; Luo et al. 2020), ability to recur (e.g., Spitler et al. 2016; CHIME/FRB Collaboration et al. 2019), and frequent association with star-forming host galaxies (Tendulkar et al. 2017; Bhandari et al. 2020; Heintz et al. 2020; Li & Zhang 2020; Mannings et al. 2020; Safarzadeh et al. 2020; Bochenek et al. 2020b). Magnetar models also received support by the discovery of an FRB-like

Corresponding author: Navin Sridhar
navin.sridhar@columbia.edu

* NASA Einstein Fellow

radio burst from the Galactic magnetar SGR1935+2154 (The CHIME/FRB Collaboration et al. 2020; Bochenek et al. 2020a) in coincidence with a luminous, hard X-ray flare (e.g., Mereghetti et al. 2020; Li et al. 2020).

Despite these many successes, magnetar models are not without challenges, and some degree of "unnaturalness":

- No confirmed magnetars (of the kind regularly observed in our Galaxy and Local Group) are sufficiently active to explain the best-studied recurring FRB sources, such as FRB 121102 (e.g., Spitler et al. 2016) or the population of repeaters discovered by CHIME/FRB (e.g., CHIME/FRB Collaboration et al. 2019). This is despite the fact that similarly active repeaters likely contribute a significant fraction of the total FRB rate, including the (currently) non-repeating population (Margalit et al. 2020; Lu et al. 2020). Such behavior may be explained by invoking a younger and/or more active magnetar population, possibly with even stronger internal magnetic fields than those of known Galactic magnetars (e.g., Beloborodov 2017). This required source population could be the product of one or more distinct, rare formation channels (e.g., exotic SNe, binary neutron star or neutron star-white dwarf mergers, or accretion-induced collapse of a white dwarf; Metzger et al. 2017; Margalit et al. 2019; Zhong & Dai 2020; Margalit et al. 2020), but these possibilities currently reside in the realm of speculation.

- The two best-studied repeating sources, FRB 180916 and FRB 121102, show periodicities in their burst arrival times of ∼16 and ∼160 days, respectively (Chime/Frb Collaboration et al. 2020; Rajwade et al. 2020). Again, several plausible ideas were proposed to generate periodic behavior within magnetar scenarios (precession, binarity, extremely slow rotation; Lyutikov et al. 2020; Beniamini et al. 2020; Levin et al. 2020; Zanazzi & Lai 2020; Li & Zanazzi 2021). However, these would all be novel, as no confirmed magnetars exhibit these properties.

- Magnetar activity is ultimately limited by the energy contained in their strong magnetic fields. This budget may become strained once realistic radiative efficiencies for the FRB emission (e.g., Plotnikov & Sironi 2019; Chen et al. 2020) are combined with the long observed active lives of some repeating sources (approaching a decade for FRB 121102; Cruces et al. 2021).

- The location of the nearest repeating source, FRB 180916, is significantly offset in its host galaxy from the nearest region of active star formation (Tendulkar et al. 2020). While consistent with the demographics of larger FRB samples (e.g., Mannings et al. 2020; Heintz et al. 2020), this location is in tension with scenarios that invoke young (age $\lesssim 10$ kyr) magnetars formed in core collapse supernovae (Tendulkar et al. 2020).

Even within the umbrella of magnetar scenarios, there exist distinct models which invoke different physical mechanisms and emission regions for generating the FRB emission (e.g., Zhang 2020a for a review). These can be broadly divided into "magnetospheric" scenarios (in which the emission originates close to the neutron star surface; Kumar et al. 2017; Kumar & Bošnjak 2020; Wadiasingh & Timokhin 2019; Wadiasingh et al. 2020) and "shock" scenarios (in which the emission originates in a relativistic outflow at much greater distances; Lyubarsky 2014; Beloborodov 2017; Plotnikov & Sironi 2019; Metzger et al. 2019; Lyubarsky 2020).

Although magnetospheric scenarios are likely exclusive to neutron star engines, shock scenarios could be applied to a wider range of central engine models. As emphasized by Metzger et al. (2019), a basic requirement of the latter is simply the impulsive injection of ultra-relativistic energy into a strongly magnetized medium of the appropriate density (one example being the relativistic wind from the terminal stage of a binary neutron star merger; Sridhar et al. 2021). Models in which FRBs are powered by magnetic reconnection in a relativistic magnetized outflow (e.g., Philippov et al. 2019; Lyubarsky 2020) could be similarly agnostic to a magnetar being the specific engine generating the triggering energy source.

All of this motivates us to look beyond magnetars, to seriously consider other central engines, whose more continuous activity, longer (e.g., binary orbital related) timescales, and greater energy reservoirs, may be more natural features. An obvious candidate, explored in this paper, are *accreting* stellar-mass compact objects, such as neutron stars (NS) or black holes (BH), which are well known to generate energetic and dynamical activity powered by strong magnetic fields carried in or generated by the accretion flow. Accretion-powered FRB engines of this broad class were previously discussed by Waxman (2017) and Katz (2017). As will become clear, the dual requirements to account for observed FRB timescales and luminosities, will drive us to the regime of super-Eddington accretion, for which the closest known observational analogs are the "ultra-luminous X-ray" sources (ULX; see Kaaret et al. 2017 for a re-
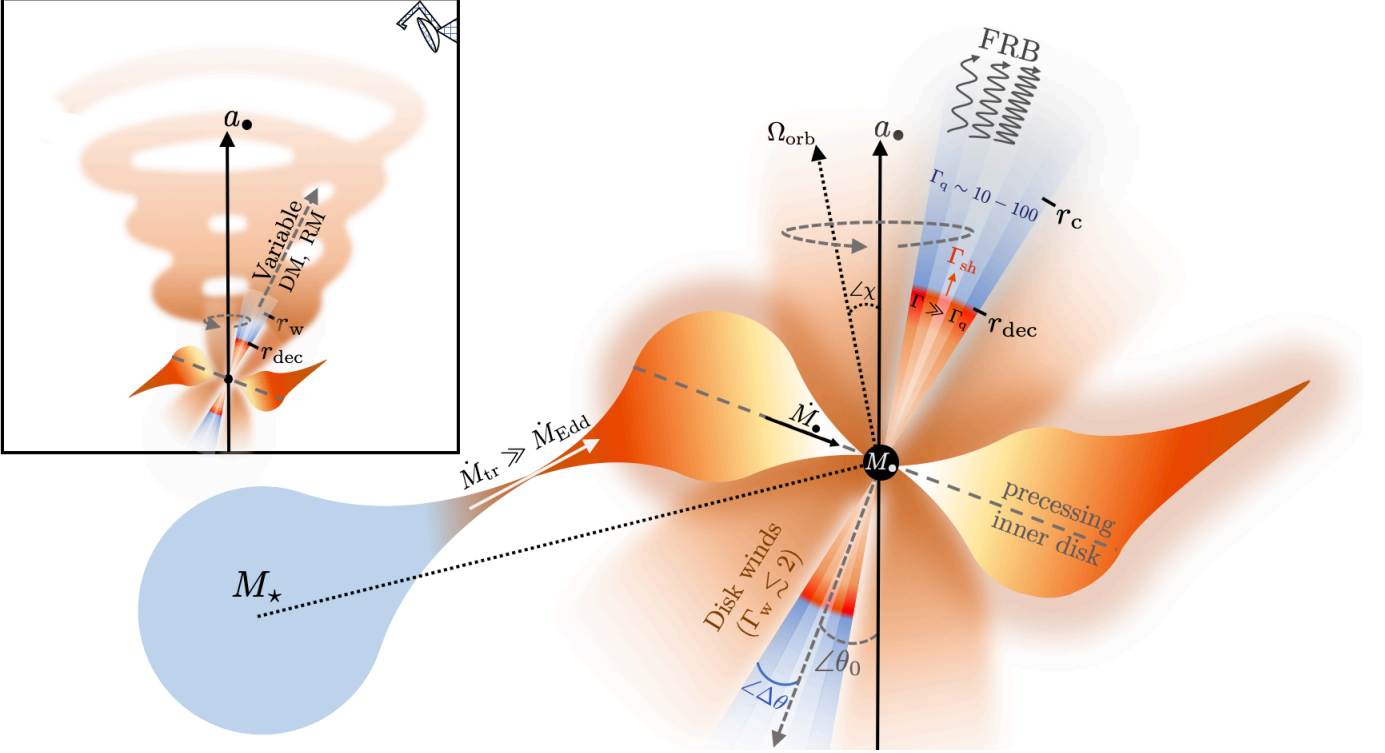
Figure 1: Schematic diagram of the production of periodic FRBs from accretion-powered flares in ULX-like binaries outlined in this paper. A star of mass $M_\star$ undergoes thermal- or dynamical-timescale mass-transfer onto a compact BH or NS remnant of mass $M_\bullet$ at rate $\dot{M}_{\rm tr}$ near or exceeding the Eddington rate. The super-Eddington accretion flow is radiatively-inefficient and hence subject to powerful outflows, which can reduce the accretion rate reaching the central compact object, $\dot{M}_\bullet \ll \dot{M}_{\rm tr}$. The mass-loaded disk winds also shape the narrow polar accretion funnel of half-opening angle $\Delta\theta$ and corresponding beaming fraction $f_{\rm b}$. FRB emission is generated by a relativistic flare of energy released close to the innermost stable circular orbit (e.g. due to reconnection of magnetic field lines threading the BH horizon), which propagates outwards along the accretion funnel as an ultrarelativistic shock into the cavity of the previous "quiescent" jet. Coherent radio emission (the FRB) is generated via the synchorotron maser shock mechanism or magnetic reconnection within the relativistic flow (at radii $\gg r_{\rm c}$, above which induced Compton scattering in the quiescent jet is negligible; eq. 8). If the spin axis of the BH is misaligned with respect to the angular momentum axis of the accretion disk, the polar cavity—and hence the direction along which the FRB emission is geometrically beamed—is modulated by Lens-Thirring precession on a timescale of days to years (eq. 27). *Inset:* The magnetized disk outflows are swept into a spiral pattern due to the precession of the disk angular momentum about the axis of BH spin ($a_\bullet$). The instantaneous jet axis intersects this wind (from an earlier precession phase) on larger scales $\gtrsim r_{\rm w}$ (eq. 33). Small systematic variations in the burst DM and RM are expected due to this encounter (eq. 35).

view). As we proceed, we shall therefore draw connections between the phenomenology of FRBs and ULX sources.

This paper is organized as follows. Section 2 begins by placing basic constraints on accretion scenarios and then moves on to outline a potential FRB mechanism. In Section 3 we discuss constraints on the types of binary systems which may give rise to the requisite accretion rates and source formation rates. Section 4 outlines additional predictions of the scenario such as host galaxies and multi-wavelength counterparts. In Section 5 we summarize predictions of the scenario and conclude. Figure 1 shows a schematic diagram of the envi-

sioned scenario, which may be helpful to refer to as we proceed.

2. BASIC CONSTRAINTS

This section considers the characteristics that an accreting central engine must satisfy in order to explain the basic observed properties of FRBs.

Consider a compact object (fiducially a BH) of mass $M_\bullet$ accreting at a rate $\dot{M}_\bullet$, which we shall normalize to the Eddington accretion rate as $\dot{m} \equiv \dot{M}_\bullet/\dot{M}_{\rm Edd}$, where $\dot{M}_{\rm Edd} \equiv L_{\rm Edd}/c^2$, $L_{\rm Edd} = 4\pi G M_\bullet c/\kappa_{\rm es}$ is the Eddington luminosity, and we take $\kappa_{\rm es} = 0.38$ cm^2 g^{-1} for the electron scattering opacity.

2.1. Timescale

The characteristic minimum timescale for significant energy release from a BH engine is set by the light crossing time of the innermost stable circular orbit:

$$t_{\min} \sim \frac{R_{\rm isco}}{c} \approx 0.3 \,{\rm ms} \; \left(\frac{m_\bullet}{10}\right) \left(\frac{R_{\rm isco}}{6R_{\rm g}}\right) \qquad (1)$$

where $R_{\rm g} \equiv GM_\bullet/c^2$. A similar expression holds in the case of a NS accretor with $R_{\rm isco}$ replaced by the NS radius, $R_{\rm NS} \simeq 12$ km (equivalent to $6R_{\rm g}$ for $M_\bullet = 1.4M_\odot$).

It may not be obvious *a priori* that the timescale over which the engine releases energy would match that of an observed FRB, but this turns out to be approximately true in emission models which invoke dissipation within a transient relativistic outflow (Section 2.5). Generic arguments suggest that FRBs must be produced in ultrarelativistic outflows (e.g. Lu & Kumar 2018). Consider a relativistically expanding ejecta shell, emitted as a "flare" from the central engine over a timescale $t_{\rm f} \gtrsim t_{\min}$ with a corresponding thickness $\Delta \simeq c \cdot t_{\rm f}$, moving outwards towards the observer with a bulk Lorentz factor $\Gamma \gg 1$. Any process which taps into the ejecta shell's energy by crossing it at close to the speed of light in the comoving frame (e.g., a reverse shock or magnetic reconnection) will complete once the shell reaches a radius $r_{\rm FRB} \sim \Gamma^2 \Delta$. Electromagnetic radiation (e.g., an FRB) which is emitted coincident with this energy release will arrive to an external observer over a timescale $\lesssim r_{\rm FRB}/2\Gamma^2 \sim t_{\rm f}$, i.e. roughly matching the original activity time of the central engine[1] (see Beniamini & Kumar 2020 for more details). This follows a similar faithful mapping between engine and prompt emission activity in gamma-ray bursts (e.g., Kumar & Zhang 2015).

2.2. Luminosity

The power of the ultra-relativistic component of a BH outflow is given by the Blandford & Znajek (1977, BZ) jet luminosity, which can be written as (Tchekhovskoy et al. 2010)

$$L_{\rm BZ} = \eta \dot{M}_\bullet c^2 \approx \eta \dot{m} L_{\rm Edd}, \qquad (2)$$

where the jet efficiency η depends on the magnetic flux threading the BH horizon and the dimensionless BH spin, $a_\bullet$. The maximum allowed $\eta = \eta_{\max}$ corresponds to a magnetically-arrested accretion disk (MAD), and

varies from $\eta_{\max} = 0.3$ for $a_\bullet \approx 0.5$ to $\eta_{\max} = 1.4$ for $a_\bullet = 0.99$ (Tchekhovskoy et al. 2011). A similar jet luminosity can in principle be generated by an accreting NS, although the magnetic flux in this case corresponds to that of the NS surface field and the dependence of the jet power on accretion rate is more complicated (e.g., Parfrey et al. 2016).

Even in the absence of a large-scale magnetic field of fixed polarity threading the disk, a temporary jet with a power $\sim L_{\rm BZ}$ can be generated by inflating and opening up small-scale field lines connecting the BH, due to the differential rotation of the accretion flow (e.g., Parfrey et al. 2015; Ripperda et al. 2019; Mahlmann et al. 2020). The instantaneous BZ jet efficiency can therefore in principle also approach $L_{\rm BZ}$ with $\eta \sim \eta_{\max} \sim 1$ for brief intervals in relatively weakly magnetized disks, the difference with the MAD case being that the mean power corresponding to the persistent jet (when the flux from a reconnected magnetic loop is not threading the BH) may be significantly lower. The "transient" nature of such a jet is an important ingredient in generating an observable FRB signal (Section 2.5).

Insofar that FRB sources turn out to be rare compared to the super-Eddington accreting BH/NS population as a whole (Section 3.2) they are allowed to represent the most extreme cases found in nature (Section 3.2) and taking $\eta \sim \eta_{\max} \sim 1$ may be justified for their most luminous bursts. The maximum isotropic radio luminosity of an FRB powered by accretion can thus be approximated as

$$L_{\rm FRB}^{\max} \approx f_\xi f_{\rm b}^{-1} \eta_{\max} \dot{M}_\bullet c^2 \sim f_\xi f_{\rm b}^{-1} \dot{m} L_{\rm Edd}$$

$$\underset{\dot{m}\gg 10}{\approx} 0.014 \left(\frac{f_\xi}{10^{-3}}\right) \left(\frac{\dot{m}}{10}\right)^3 L_{\rm Edd}, \qquad (3)$$

where $f_\xi \equiv L_{\rm FRB}/L_{\rm BZ}$ is the efficiency of converting the transient jet's energy into coherent radio emission (e.g., $f_\xi < 10^{-2}$ in synchrotron maser scenarios; Section 2.5) and $f_{\rm b}$ is the beaming fraction. The final line in equation (3) employs an expression for the X-ray beaming fraction motivated by ULX observations (eq. 4), an appropriate choice if the FRB is geometrically beamed along the narrow accretion funnel (Section 2.3).

Figure 2 shows the observed durations and luminosities of a large sample of FRBs, including the well-studied repeating sources FRB 121102 and FRB 180916. The top axis gives the value of $M_\bullet$ corresponding to $t_{\min}$ (eq. 1) for $R_{\rm isco} \simeq 2R_{\rm g}$ (a rough lower limit corresponding to a rapidly spinning BH). Colored contours show the corresponding minimum Eddington ratio $\dot{m}$ required to achieve $L_{\rm FRB} = L_{\rm FRB}^{\max}$ (eq. 3) for an assumed efficiency $f_\xi = 10^{-3}$ using the value $M_\bullet$ corresponding to the $t_{\min}$ condition (Section 2.5). The contours are de-

---

[1] In FRB emission models powered by a shock propagating into a high magnetization $\sigma \gg 1$ medium, the observed emission duration can be shorter than that of the engine (e.g. Babul & Sironi 2020).
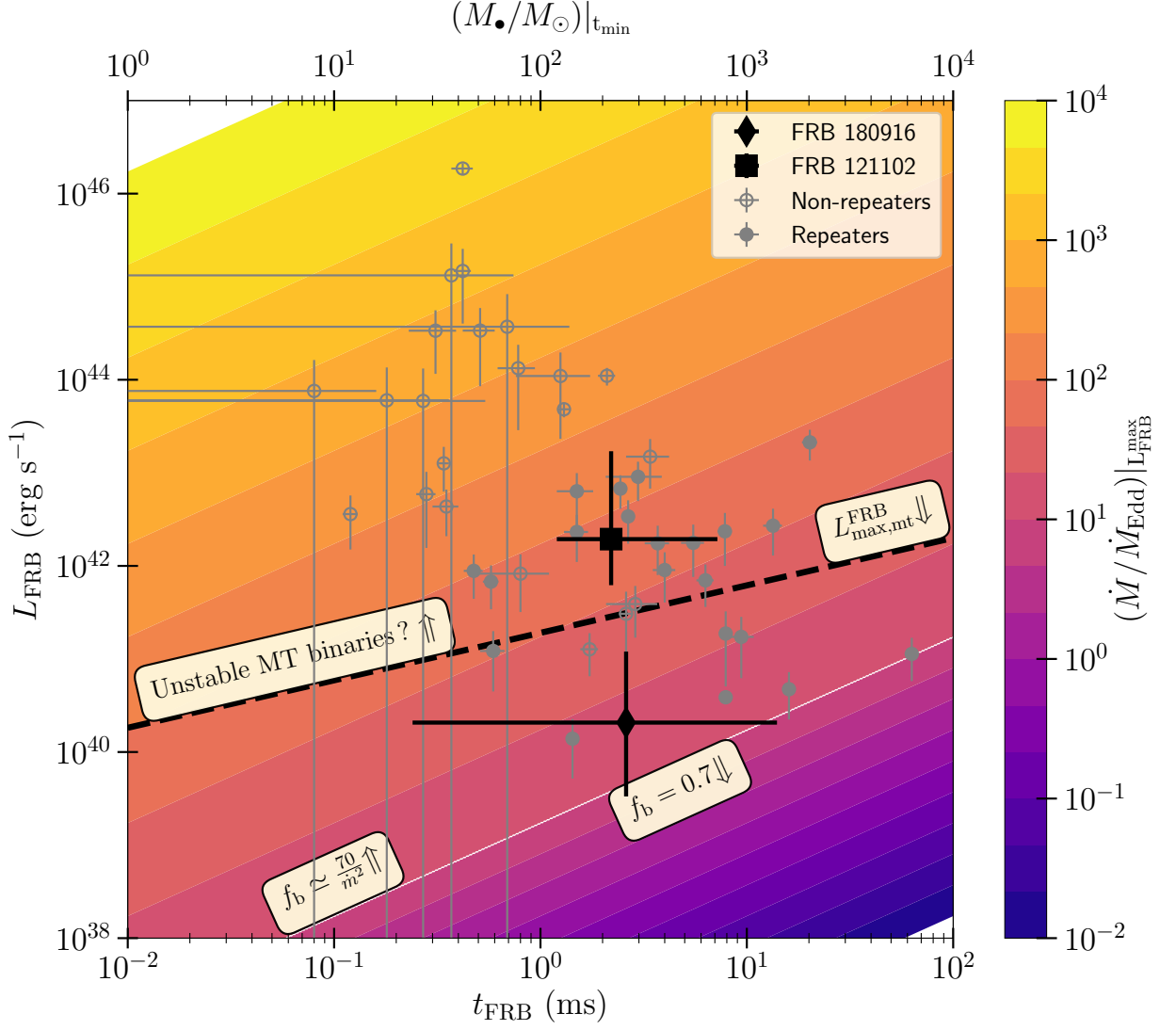
Figure 2: If FRBs are powered by accreting compact objects, the latter must be a NSs or stellar-mass BHs accreting near or well above the Eddington rate. Here we show the observed luminosities and durations of repeating and non-repeating FRBs as filled and non-filled grey circles, including ranges for the repeating sources, FRB 121102 (square) and FRB 180916 (diamond) (http://www.frbcat.org; Petroff et al. 2016, and the references therein). The top axis shows the NS/BH mass $M_\bullet$ corresponding to the minimum FRB duration $t_{\min}$ (eq. 1) assuming $R_{\rm isco} = 2R_{\rm g}$. Colored contours show the corresponding mass transfer Eddington ratio required to achieve $L_{\rm FRB} = L_{\rm FRB}^{\max}$ (eq. 3) for an assumed FRB emission efficiency $f_\xi = 10^{-3}$ (Section 2.5) using the value $M_\bullet$ corresponding to the $t_{\min}$ condition and adopting a beaming fraction motivated by ULX observations (eq. 4). A dashed black line shows the limit corresponding to systems undergoing stable mass-transfer (MT) accretion (eq. 21).

rived by assuming the beaming fraction motivated by ULX observations (eq. 4 and surrounding discussion).

Firstly, we see that observed FRB durations require accretors of mass $M_\bullet \lesssim 10 - 10^3 M_\odot$, corresponding to NSs or stellar-mass BHs. Also note that in order to explain the most luminous FRBs (particularly the non-repeating sources) we require super-Eddington accretion

rates, $\dot{m} \gtrsim 1 - 10^3$. Section 3 describes the stellar binary systems needed to generate such high accretion rates.

2.3. Beaming

Fig. 2 demonstrates that the most luminous FRB sources require accretion rates $\dot{m} \gg 1$. Such super-Eddington levels of accretion (Shakura & Sunyaev 1973) correspond to the regime of photon-trapped radiatively

inefficient accretion flows (RIAF; e.g., Abramowicz et al. 1988; Narayan & Yi 1995; Blandford & Begelman 1999). These systems are characterized by optically- and geometrically-thick accretion disks with powerful mass-loaded winds (e.g. Begelman et al. 2006; Poutanen et al. 2007) and a narrow open funnel along the polar axis defined by the disk angular momentum. Super-Eddington accretion is likely responsible for at least some of the ULX population, even when the accretor is a magnetized NS (Bachetti et al. 2014; Mushtukov et al. 2015).

To reproduce observed properties of ULX, King (2009) estimate a geometric beaming fraction for the X-ray emission, corresponding to the opening solid angle of the accretion funnel, given by

$$f_{\rm b,X} \approx \begin{cases} 0.7, & \dot{m} \ll 10 \\ \frac{73}{\dot{m}^2}, & \dot{m} \gg 10 \end{cases}, \qquad (4)$$

where the specific constant value of 0.7 in the $\dot{m} \ll 10$ limit is chosen for continuity with the $\dot{m} \gg 10$ limit. Given the requirements of an extremely clean environment to generate an observable FRB (Section 2.4), the relativistic outflow responsible for powering the FRB will itself likely be confined to a similar solid angle (Fig. 1). In such a case, $f_{\rm b,X}$ provides at least an upper limit on the beaming fraction of the FRB itself, $f_{\rm b}$.

In Section 3.3 we describe a scenario in which periodic FRB activity results from precession of the accretion disk's polar funnel (of half-opening angle $\Delta\theta$ and corresponding $f_{\rm b}$) across our line of sight (see also Katz 2017, who propose a similar geometry). In this case, taking $f_{\rm b} = 2\pi(\Delta\theta)^2/(4\pi)$, the FRB duty cycle is then given by:

$$\zeta \approx \frac{\Delta\theta}{2\pi\theta_0} \approx \left(\frac{f_{\rm b}}{2\pi^2\theta_0}\right)^{1/2} \approx \begin{cases} \frac{0.19}{\theta_0^{1/2}} & \dot{m} \ll 10 \\ \frac{1.9}{\dot{m}\theta_0^{1/2}}, & \dot{m} \gg 10 \end{cases} \qquad (5)$$

where θ_0 is the angle of the axis of precession makes with respect to the observer's line of sight. The observed duty cycle $\zeta \approx 0.3 - 0.35$ of FRB 180916 (Chime/Frb Collaboration et al. 2020), or $\zeta \approx 0.55$ for FRB 121102 (Rajwade et al. 2020), would then imply $\dot{m}\theta_0^{1/2} \lesssim 4 - 6$. For values $\theta_0 \lesssim 0.1 - 1$, the implied accretion rates $\dot{m} \gtrsim 10$ are broadly consistent with those required to power the burst luminosities from these sources (Fig. 2).

2.4. Clean Environment for FRB Escape

Various physical processes can absorb or attenuate radio waves in the vicinity of an accreting compact object. One of the most severe is induced Compton scattering of the FRB beam by electrons surrounding the source (e.g., Lyubarsky 2008). This makes it highly non-trivial

to find the clean environment needed for the FRB to escape to an observer at infinity, given the dense outflows present in super-Eddington accretion systems. The only plausible scenario is for the emission generated at large radii, far from the original launching point of the flare, by relativistically expanding material directed outwards along the narrow polar accretion funnel (which prior to the FRB-generating flare carried only the comparatively low-density jet, uncontaminated by the mass-loaded disk outflows present at wider angles).

At the onset of the FRB-generating flare, the polar accretion funnel is filled by the plasma of whatever jet of lower power $L_{\rm q} = \eta_{\rm q} L_{\rm BZ}$ was present just prior to the flare, where here $\eta_{\rm q} \lesssim 1$ is the efficiency of the steady "quiescent" jet relative to that of the higher power $L_{\rm BZ} \sim \eta \dot{M}_\bullet c^2$ of the transient outburst responsible for powering the FRB (eq. 2). Below, we discuss different physical interpretations of the low $\eta_{\rm q} \ll 1$ medium, such as whether it truly indicates a less efficient jet (at the same accretion rate, $\dot{M}_\bullet$), or just a much lower $\dot{M}_\bullet$.

The lab-frame electron density of the quiescent jet at radius r from the compact object is given by

$$n_q = \frac{\eta_{\rm q} L_{\rm BZ}}{4\pi(1+\sigma_{\rm q})f_b \Gamma_{\rm q} m_p c^3 r^2}, \qquad (6)$$

where $\sigma_{\rm q}$ and $\Gamma_{\rm q}$ are the magnetization and bulk Lorentz factor of the quiescent jet, respectively, and we have assumed an electron-ion jet composition.[2]

The optical depth to induced electron scattering above a radius r in the wind, for an FRB of luminosity $L_{\rm FRB}$, duration $t_{\rm FRB}$, and frequency $\nu_{\rm FRB}$, is approximately given by (Lyubarsky 2008; Metzger et al. 2019)

$$\tau_{\rm c} \sim \frac{3}{320\pi^2} \frac{\sigma_T}{m_e} \frac{L_{\rm FRB} \cdot ct_{\rm FRB} \cdot n_q}{\nu_{\rm FRB}^3 r^2} \cdot \Gamma_{\rm q}^3, \qquad (7)$$

where $\sigma_{\rm T}$ is the Thomson cross section and the factor of $\Gamma_{\rm q}^3$ follows from the relativistic transformation of the induced scattering optical depth from the rest-frame of the upstream wind (Margalit et al. 2019).[3]

Substituting equation (6) with $L_{\rm q} = \eta_{\rm q} L_{\rm FRB} f_{\rm b}/f_\xi$ into equation (7) we find that $\tau_{\rm c} \lesssim 1$ is achieved at

---

[2] The composition of a BH or NS jet is likely to be dominated by electron/positron pairs on small scales close to the compact object (e.g. Globus & Levinson 2013). However, by the larger radial scales of interest the quiescent jet may have entrained baryons from the jet walls defined by the surrounding disk wind.

[3] An additional complication can arise from the impact of the strong wave of the FRB in accelerating the electrons in the upstream scattering medium to relativistic speeds. However, Margalit et al. (2019) show that the enhancement in the optical depth due to this effect is cancelled by the suppression of the scattering rate of the relativistic electrons found by Lyubarsky (2019).

radii satisfying

$$r \gtrsim r_{\rm c} \approx \left[\frac{3\sigma_{\rm T}\eta_q L_{\rm FRB}^2 t_{\rm FRB}\Gamma_q^2}{1280\pi^3 m_e m_p c^2 \nu_{\rm FRB}^3 f_\xi} \right]^{1/4}$$

$$\approx 8 \times 10^{13}{\rm cm}\, \frac{L_{40}^{1/2} t_{-3}^{1/4}\Gamma_{q,2}^{1/2}}{\nu_9^{3/4} f_{\xi,-3}^{1/4}}\frac{\eta_{q,-3}^{1/4}}{(1+\sigma_{\rm j})^{1/4}}, \qquad (8)$$

where $\eta_{q,-3} \equiv \eta_q/(10^{-3})$, $\Gamma_{q,2} = \Gamma_q/100$, $\nu_9 = \nu_{\rm FRB}/10^9{\rm Hz}$, $L_{40} \equiv L_{\rm FRB}/10^{40}{\rm erg\,s^{-1}}$, $t_{-3} \equiv t_{\rm FRB}/1\,{\rm ms}$, $f_{\xi,-3} \equiv f_\xi/10^{-3}$.

To produce an FRB of duration $t_{\rm FRB} \sim r_{\rm FRB}/(2\Gamma^2 c)$ at radius $r_{\rm FRB} > r_{\rm c}$, the Lorentz factor Γ of the emitting region must obey

$$\Gamma > \Gamma_{\rm min} \approx \left(\frac{r_{\rm c}}{2ct_{\rm FRB}} \right)^{1/2} \approx 400 r_{c,13}^{1/2} t_{-3}^{-1/2}, \qquad (9)$$

where $r_{c,13} \equiv r_{\rm c}/(10^{13}{\rm cm})$ and we have assumed a mildly magnetized upstream $\sigma_{\rm j} \lesssim 1$. The Thomson depth from the emission radius $r_{\rm FRB} > r_{\rm c}$ through the quiescent outflow at large radii is given by

$$\tau_{\rm T} \simeq \int_{r_{\rm FRB}}^\infty n_q\sigma_{\rm T}dr \approx \frac{\eta_q L_{\rm BZ}\sigma_{\rm T}}{4\pi f_b\Gamma_q m_e c^3 r_{\rm FRB}(1+\sigma_{\rm j})}$$

$$\approx 3 \times 10^{-8}\frac{m_\bullet}{10}\frac{r_{\rm c}}{r_{\rm FRB}}\frac{\eta\dot{m}}{r_{c,13}f_{b,-1}\Gamma_{q,2}}\frac{\eta_{q,-3}}{(1+\sigma_{\rm j})} \quad (10)$$

and the corresponding dispersion measure (DM),

$$DM[{\rm pc\,cm^{-3}}] \simeq 5 \times 10^5 \frac{\tau_{\rm T}\Gamma_q}{(1+z)}$$

$$\approx \frac{1.6}{(1+z)}\frac{r_{\rm c}}{r_{\rm FRB}}\frac{m_\bullet}{10}\frac{\eta\dot{m}}{r_{c,13}f_{b,-1}}\frac{\eta_{q,-3}}{(1+\sigma_{\rm j})}, \qquad (11)$$

where z is the source redshift.

In addition to requiring an FRB be freely able to propagate to Earth ($\tau_{\rm c} < 1$), one must also not overproduce the measured local DM value or its time variation between bursts from the same source, ΔDM (for example, ΔDM $\lesssim 2$ pc cm^{-3} in FRB 180916; Chime/Frb Collaboration et al. 2020). Equations (8)-(11) reveal that satisfying both of these conditions is possible, but it likely requires (1) the FRB being generated by a highly relativistic outflow, $\Gamma \gg 100$, (2) which propagates into the medium corresponding to a jet of extremely low luminosity, $\eta_q \ll 10^{-2}$ and/or one with a very high magnetization $\sigma_{\rm j} \gg 1$. The next section describes how similar requirements emerge within a specific FRB emission model. Figure 3 summarizes the allowed parameter space of quiescent jet properties needed to simultaneously satisfy constraints on the shock emission radius ($r_{\rm dec} > r_{\rm c}$) and on the lack of local time-variable DM contribution due to propagation through the jet.

Can accreting stellar-mass compact objects generate outflows with $\Gamma > 100$? The jets of Galactic X-ray binaries are inferred from observations to achieve Lorentz factors of at least a few to tens (e.g., Mirabel & Rodríguez 1994; Fender et al. 2004), although the constraints are model dependent and generally amount to lower limits (Miller-Jones et al. 2006). As in AGN jets, radiative acceleration of optically thin gas to relativistic velocities is severely limited by radiation drag effects (e.g. Phinney 1982); however, these effects are reduced if the flow entrains a large enough optical depth in ambient matter to shield itself. From radiation acceleration alone, Begelman (2014) argues that jets from super-Eddington accretion systems can achieve $\Gamma \simeq \dot{m}^{1/4}$, corresponding to $\Gamma \gtrsim 5$ for $\dot{m} \gtrsim 10^3$. Even higher Lorentz factors can be achieved by acceleration resulting from magnetic dissipation of a high-σ flow in an optically-thick environment (e.g., Drenkhahn & Spruit 2002). An extreme limit are gamma-ray burst jets, which attain $\Gamma \gtrsim 100 - 1000$ (e.g. Lithwick & Sari 2001). Taken together, it does not seem excluded that systems undergoing highly super-Eddington accretion (unlike the vast majority of X-ray binaries in our Galaxy) are capable for brief periods of generating sufficiently relativistic outflows to satisfy the constraints (9), (11).

We also require a low effective efficiency $\eta_q \ll 1$, and/or large magnetization $\sigma_{\rm j} \gg 1$, in the quiescent jet. One way to generate a large contrast in jet power between the quiescent and an FRB-generating flaring state would be through a sudden ($\sim$ dynamical timescale) large increase in the mass accretion rate reaching the central object. This could achieved, for example, by a highly magnetized NS accretor transitioning between a state of steady accretion and a "propellor" regime in which accretion is prohibited (e.g. Parfrey & Tchekhovskoy 2017). Although sufficiently large changes in the accretion rate (up to a factor $\sim 10^3$) are observed in Galactic X-ray pulsars (Tsygankov et al. 2016), the frequency of mode-switching would need to be much more rapid than is observed to explain the most active recurring FRBs, which exhibit interburst intervals as short as $\sim 10-100$ s (e.g., Gourdji et al. 2019). Large amplitude changes in the accretion rate are also inferred in ULX (Kaaret & Feng 2009; Bachetti et al. 2014) and from the class of low-mass X-ray binaries known as soft X-ray transients (e.g., Tanaka & Shibazaki 1996), but again over much longer timescales much than needed to explain actively recurring FRB sources.

Even for a constant accretion rate $\dot{M}_\bullet$, a rise in the jet efficiency $\eta \propto \Phi_{\rm B}^2$ can be driven by an increase in the magnetic flux $\Phi_{\rm B}$ threading the BH horizon. Although one has $\eta = \eta_q \sim \mathcal{O}(1)$ for the jet of a spinning BH in a

persistently MAD state (Tchekhovskoy et al. 2010), long phases of $\eta_q \ll 1$ could be possible if the inner disk only irregularly receives a large magnetic flux bundle (Spruit & Uzdensky 2005; Parfrey et al. 2015).

Finally, the above constrains could also be satisfied even for a relatively constant jet power ($\eta_q \sim 1$) if the quiescent jet is extremely highly magnetized $\sigma_j \gg 1$ (and hence low density) relative to the FRB generating flare.

2.5. Emission Mechanism

Advancing beyond the basic considerations of the previous section requires the identification of a specific emission mechanism capable of converting a sudden release of relativistic energy from the engine ("flare") into coherent radio emission at radii $r_{\rm FRB} \gg r_c \sim 10^{13}$ cm. One such mechanism, which we focus on for concreteness, is synchrotron maser emission from the relativistic shock generated as flare ejecta from the central engine collides with a magnetized upstream (Lyubarsky 2014; Beloborodov 2017; Metzger et al. 2019; see also Waxman 2017). In the present context, the upstream medium is the "wind" of the quiescent jet.

Plasmoid mergers induced by magnetic reconnection in the current sheets of BH magnetospheres (e.g. Philippov et al. 2019; Lyubarsky 2020), or induced reconnection in the striped high-σ_j quiescent jet (and resulting inverse turbulent cascade; Zrake & Arons 2017), provide a potential alternative emission mechanism for the flare. However, we note that the conditions for an FRB to escape from the relativistically hot plasma are generally more severe than from a cold upstream (Lyubarsky 2008).

Returning to the shock scenario, consider an accretion flare, which releases a transient ultra-relativistic outflow of luminosity $L_f \sim \eta \dot{M}_\bullet c^2$ (eq. 2), duration $t_f \sim t_{\rm min}$ (eq. 1), and radial bulk Lorentz factor $\Gamma_f \gg \Gamma_{\rm min}, \Gamma_q$. Such flare ejecta could represent a magnetized plasmoid generated by a powerful reconnection event close to the BH/NS magnetosphere or light cylinder (e.g., Parfrey et al. 2015; Ripperda et al. 2019; Yuan et al. 2020). The flare ejecta will sweep up gas in the pre-existing quiescent jet (eq. 6), transferring it to a forward shock by a radius (Sari & Piran 1995)

$$r_{\rm dec} \approx 2\Gamma_{\rm sh}^2 c \cdot t_f \approx 2 \times 10^{13} \eta_{q,-3}^{-1/2} t_{f,-3} \Gamma_{q,2}^2 \, {\rm cm}, \quad (12)$$

where (Beloborodov 2017)

$$\Gamma_{\rm sh} \simeq \Gamma_q \left(\frac{L_f}{L_q}\right)^{1/4} \simeq \frac{\Gamma_q}{\eta_q^{1/4}} \approx 560 \frac{\Gamma_{q,2}}{\eta_{q,-3}^{1/4}}, \quad (13)$$

is the Lorentz factor of the shocked gas during the initial deceleration phase. As discussed in the previous section, in order for the deceleration−and concomitant radio emission−to occur in an optically thin environment ($r_{\rm dec} \gg r_c$; eq. 8) we require a large Lorentz factor of the quiescent jet $\Gamma_q \gtrsim 100$ and/or an extreme contrast $\eta_q \lesssim 10^{-3}$, between the jet luminosity during the flare and that of prior quiescent state (Fig. 3).

The synchrotron maser emission peaks at a frequency (e.g., Beloborodov 2017; Plotnikov & Sironi 2019)

$$\nu_{\rm pk} \sim \frac{3\Gamma_{\rm sh} c}{2\pi r_{\rm L}} \sim \frac{3e(L_f L_q)^{1/4}}{2\pi m_e c^{3/2} r_{\rm FRB}} \approx \frac{e\eta^{1/2} L_{\rm Edd}^{1/2}}{4\pi m_e c^{5/2}} \frac{r_{\rm dec}}{r_{\rm FRB}} \frac{\dot{m}^{1/2} \eta_q^{3/4}}{t_f \Gamma_q^2}$$

$$\approx 1.9 \, {\rm GHz} \left(\frac{r_{\rm FRB}}{r_{\rm dec}}\right)^{-1} \left(\frac{m_\bullet}{10}\right)^{1/2} \left(\frac{\dot{m}}{10^2}\right)^{1/2} \frac{\eta^{1/2} \eta_{q,-3}^{3/4}}{\Gamma_{q,2}^2 t_{-3}} (14)$$

where $r_{\rm L} = \Gamma_q m_e c^2 / e B_q$ is the Larmor radius of electrons in the shocked plasma, $B_q \simeq (L_q \sigma_q / c r_{\rm FRB}^2)^{1/2}$ is the upstream magnetic field of the quiescent jet material at the radius $r_{\rm FRB}$ of the FRB emission assuming $\sigma_q \gtrsim 1$. The efficiency of the FRB maser emission is $f_\xi \sim 10^{-3}$ for $\sigma_q \gtrsim 1$ (Plotnikov & Sironi 2019; Babul & Sironi 2020), motivating the choice for $L_{\rm FRB}^{\rm max}$ in Fig. 2. Colored lines in Fig. 3 show the required properties of the quiescent jet to produce a burst with $\nu_{\rm pk} \sim 1$ GHz for different values of $\dot{m}$.

As described previously in the context of magnetar models, deceleration of the flare ejecta by the blast wave and its propagation to lower densities at radii $\gtrsim r_{\rm dec}$ produces downward drifting of $\nu_{\rm pk}$ and hence the frequency structure of the bursts (Metzger et al. 2019; Beloborodov 2019; Margalit et al. 2019), similar to that observed in the sub-bursts of FRB 121102 (Hessels et al. 2019) and the CHIME repeaters (CHIME/FRB Collaboration et al. 2019). For $\sigma_q \gg 1$ the bursts are (at the source) nearly 100% linearly polarized, dominated by the X-mode whose electric field is perpendicular to the upstream magnetic field and hence for a laminar quiescent jet parallel to the approximately fixed direction of the BH/NS spin vector (although for lower $\sigma_q \lesssim 1$ the shock also radiates an intense O-mode, with power nearly comparable to the X-mode, which then deteriorates the polarization degree; Iwamoto et al. 2018).

A roughly fixed polarization angle is consistent with observations of FRB 121102 (e.g. Michilli et al. 2018) but in tension with others bursts which show polarization swings across the burst duration (e.g., Luo et al. 2020; Day et al. 2020). The latter would require a more complicated magnetic field geometry in the upstream jet material than a laminar jet, for instance due to the effects of non-axisymmetric kink instabilities (e.g., Bromberg & Tchekhovskoy 2016) or the interaction of the jet with the accretion disk wind at large radii as a result of disk precession (Section 2.4).
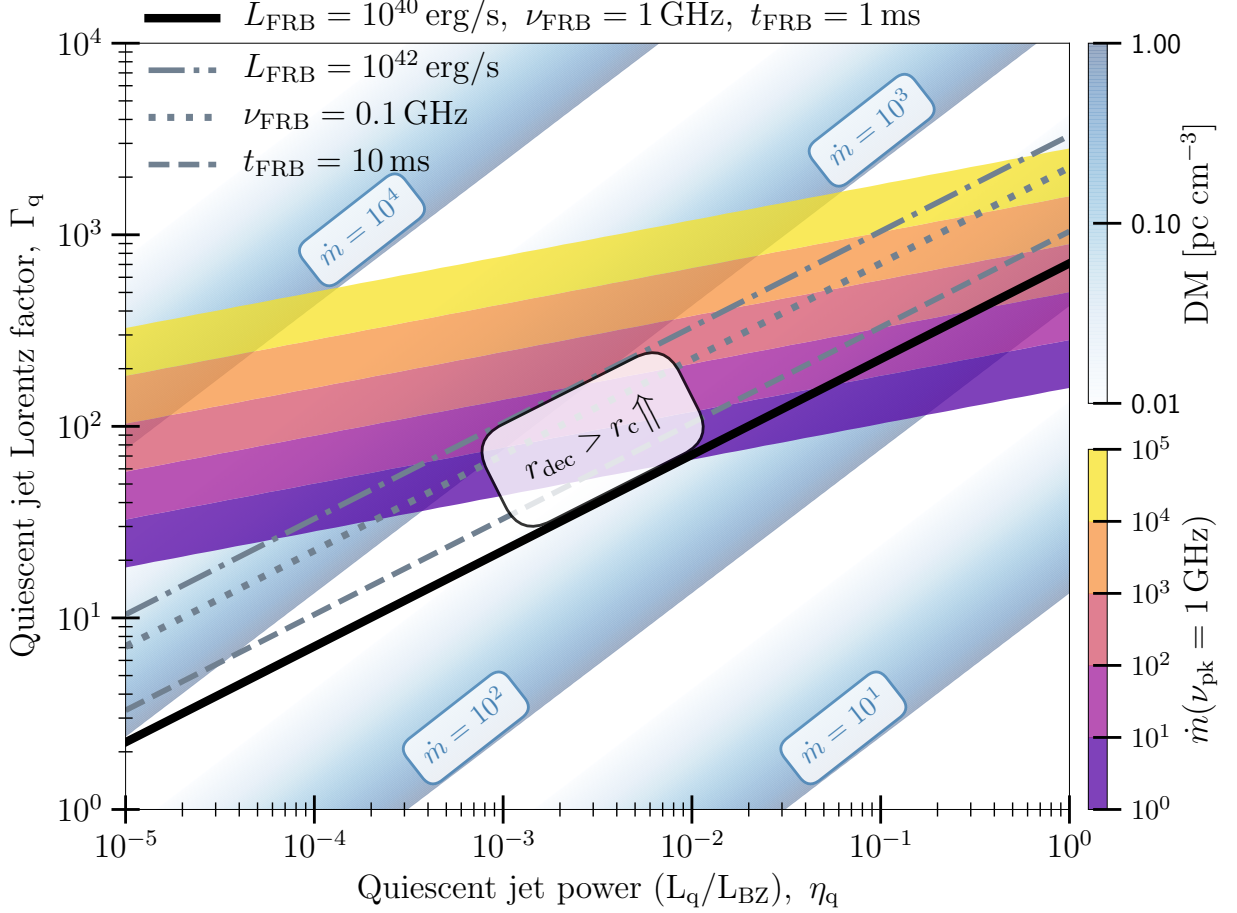
Figure 3: The quiescent jet just prior to the FRB flare must be comparatively dilute and highly relativistic. Here we show the allowed parameter space of the quiescent jet (η_q, Γ_q), based on the constraints from the optical depth for FRB escape, and on the local dispersion measure (DM) variation. The requirement of $r_{dec} > r_c$ for an optically thin upstream medium is demarcated by the diagonal lines (see eqs. 8 and 12). The solid black line corresponds to the fiducial case of an FRB with $L_{FRB} = 10^{40}\,\mathrm{erg\,s^{-1}}$, $\nu_{FRB} = 1\,\mathrm{GHz}$, $t_{FRB} = 1\,\mathrm{ms}$. The grey dash-dotted, dotted, and dashed lines each denote the deviation of the burst luminosity ($L_{FRB} = 10^{42}\,\mathrm{erg\,s^{-1}}$), frequency ($\nu_{FRB} = 0.1\,\mathrm{GHz}$), and the duration ($t_{FRB} = 10\,\mathrm{ms}$), respectively, from the "fiducial FRB". The local environmental contribution to the DM, for the fiducial FRB, corresponding to different $\dot{m} \in [10, 10^4]$, are denoted by the fading blue bands (assuming $r_{FRB} = r_{dec}$; see eqs. 11 and 12); the dark region corresponds to the expected upper limit of $\sim 1\,\mathrm{pc\,cm^{-3}}$. The values of η_q and Γ_q required to produce the fiducial FRB (with an emission peak at $\nu_{pk} = 1\,\mathrm{GHz}$), for different $\dot{m} \in [1, 10^5]$ are represented by the central yellow-violet "emission contours" (see eq. 14). For a given $\dot{m}$, the allowed range of η_q and Γ_q are set by the regions to the left of the intersection of the corresponding emission contour with the DM=1 pc cm^{-3} band, and above the $r_{dec} = r_c$ line. Throughout, we assume $\eta = 1$, $\sigma_j = 1$, $f_\xi = 10^{-3}$, flare duration $t_f \sim t_{min} = 1\,\mathrm{ms}$, redshift $z = 0$, $f_b \approx 70/\dot{m}^2$, and $m_\bullet = 10$.

3. BINARY PROPERTIES

The vast majority of accreting Galactic NS/BH sources reside in long-lived X-ray binary systems with mass transfer rates at or below the Eddington rate. However, as shown in Fig. 2, such sources are energetically strained to explain most luminous FRBs. Nevertheless, there exist more extreme systems with much higher accretion rates. These include the microquasar binary SS433 (Margon 1984; Fabrika 2004) which is likely a BH being fed by a massive late A-type companion star at a super-Eddington rate (e.g., Hillwig & Gies 2008). Such a source viewed face-on would be a

strong (and periodic due to jet precession) X-ray source perhaps akin to a ULX.[4]

One binary channel capable of generating sustained levels of highly super-Eddington accretion is stable thermal timescale mass-transfer. This can occur as an evolved massive secondary star undergoes Roche Lobe overflow, either on the main sequence (case A mass transfer) or later when crossing the Hertzsprung gap to become a giant (e.g., King & Begelman 1999; King et al. 2001; Rappaport et al. 2005; Wiktorowicz et al. 2015). As the stellar envelope becomes fully convective approaching the Hayashi track, the adiabatic response of the star to mass loss may lead to dynamically unstable mass transfer, which manifests as a "common envelope event" engulfing the system in gas and ultimately precluding the clean environment necessary for FRB formation. However, as emphasized by Pavlovskii et al. (2017), a large fraction of systems nominally in the unstable regime may in fact undergo stable mass transfer due to their outermost surface layers remaining radiative[5] (see also Marchant et al. 2017).

This section considers whether such systems can provide accreting BH/NS systems with the properties required to power FRBs as discussed thus far. We initially focus on stable mass-transfer systems, and finding it potentially insufficient to account for the most luminous FRBs, return to the shorter-lived unstable systems at the end.

3.1. *Mass Transfer Rate*

For thermal timescale mass transfer from a star of mass $M_\star = m_\star M_\odot$ in a semi-detached binary to the companion of mass $m_\bullet$ (in our case, a BH or NS), the mass transfer rate can achieve a value (e.g., Kolb 1998),

$$\dot{M}_{\rm tr} \sim \frac{M_\star}{\tau_{\rm KH}} \sim 3 \times 10^{-8} m_\star^{2.6} M_\odot {\rm yr}^{-1}, \qquad (15)$$

where

$$\tau_{\rm KH} \approx 3 \times 10^7 \frac{m_\star^2}{r_\star l_\star} {\rm yr} \approx 3 \times 10^7 m_\star^{-1.6} {\rm yr} \qquad (16)$$

is the Kelvin-Helmholtz time of the star when it leaves the main sequence and $L_\star = l_\star L_\odot$ is its luminosity. In the final lines of (15), (16), we have assumed a main-sequence star of mass $1 \lesssim m_\star \lesssim 40$ with a radiative

envelope, for which one approximately has the scaling relationships $r_\star \propto m_\star^{0.6}$ and $l_\star \propto m_\star^3$.

On the other hand, $\dot{M}_{\rm tr}$ cannot be arbitrarily large, or the super-Eddington disk cannot "fit" into the binary. More precisely, if the disk is locally super-Eddington even at the circularization radius, then a thick disk encompasses the entire system and common envelope-like runaway might still occur. King & Begelman (1999) estimate this will occur for $m_\star \gtrsim 53 m_\bullet^{0.18}$, placing an Eddington-scaled upper limit on $\dot{M}_{\rm tr}$ of

$$\frac{\dot{M}_{\rm tr}^{\rm max}}{\dot{M}_{\rm Edd}} \sim 2.6 \times 10^5 \left(\frac{m_\bullet}{10}\right)^{-0.49}. \qquad (17)$$

To power FRB emission, we are interested in the accretion rate reaching the innermost radii of the disk. However, for super-Eddington accretion only a small fraction of the transferred mass is expected to reach the BH due to massive winds (e.g. Blandford & Begelman 1999). In particular, for $\dot{M}_{\rm tr} \lesssim \dot{M}_{\rm tr}^{\rm max}$ we expect

$$\dot{M}_\bullet \simeq \dot{M}_{\rm tr} \left(\frac{R_{\rm Edd}}{R_{\rm isco}}\right)^{-p}, \qquad (18)$$

where $R_{\rm Edd} \simeq R_{\rm g} \left(\frac{\dot{M}_{\rm tr}}{\dot{M}_{\rm Edd}}\right)$ is the trapping radius interior to which the disk becomes locally super-Eddington and $p < 1$. Taking a value $p \approx 0.7$ motivated by hydrodynamical simulations of RIAFs (Yuan & Narayan 2014), we obtain

$$\dot{m} = \left(\frac{R_{\rm isco}}{R_{\rm g}}\right)^{0.7} \left(\frac{\dot{M}_{\rm tr}}{\dot{M}_{\rm Edd}}\right)^{0.3} \qquad (19)$$

The upper limit on the mass-transfer rate (17) then becomes an upper limit on the accretion rate reaching the central compact object,

$$\dot{m} \lesssim 68 \left(\frac{R_{\rm isco}}{2R_{\rm g}}\right)^{0.7} \left(\frac{m_\bullet}{10}\right)^{-0.15} \qquad (20)$$

From Equation (3), we obtain a theoretical maximum of the isotropic FRB luminosity for stably accreting sources:

$$L_{\rm FRB,mt}^{\rm max} \approx 4.4 L_{\rm Edd} f_{\xi,-3} \left(\frac{R_{\rm isco}}{2R_{\rm g}}\right)^{2.1} \left(\frac{m_\bullet}{10}\right)^{-0.45}, \quad (21)$$

where we have taken $f_{\rm b} = f_{\rm b,X}$ (eq. 4) in the $\dot{m} \gg 10$ limit (as satisfied for $m_\bullet \lesssim 10^3$ for $R_{\rm isco} \sim R_{\rm g}$).

The constraint (21) is shown as a black line in Fig. 2. Many observed FRBs can in principle satisfy the $L_{\rm FRB,mt}^{\rm max}$ limit. However, it is violated by the most luminous sources, particularly many of the (currently) non-repeating sources. These FRBs could still be powered by accreting systems if the latter are undergoing

---

[4] SS433 in fact exhibits X-ray emission with evidence for precession in the light curve (Atapin & Fabrika 2016); however, the X-rays are believed to arise from the jet rather than the accretion disk.

[5] Making such systems stable also reduces the predicted rate of binary black hole mergers from population synthesis models, bringing them into better accord with observations by LIGO/Virgo.

unstable mass transfer at a rate $\dot{M}_{\rm tr} \gg \dot{M}_{\rm tr,max}$. Such systems may have just begun mass-transfer but are in the process of evolving towards a merger or common envelope (e.g., MacLeod & Loeb 2020).

The "lifetime" of unstable systems as potential FRB sources would correspond to the timescale for runaway accretion. Based on observations and detailed modeling of the binary star merger V1309 Sco (Tylenda et al. 2011; Pejcha 2014; Pejcha et al. 2017) this evolution time can be estimated as

$$\tau_{\rm unst} \sim 5 - 100 P_{\rm orb} \sim 10 - 10^5 {\rm d}, \qquad (22)$$

where $P_{\rm orb} \sim 1 - 1000$ d is the binary orbital period (eq. 26). The resulting mass transfer rate, $\dot{M}_{\rm tr} \sim M_\star/\tau_{\rm unst} \sim 10^3 - 10^7 \dot{M}_{\rm Edd}$ (e.g., for $M_\star \sim 10 M_\odot$), can in principle exceed $\dot{M}_{\rm tr}^{\rm max}$ (eq. 17) by many orders of magnitude. Even accounting for mass-loss from disk winds this could result in accretion rates reaching the compact object $\dot{m} \gtrsim 10 - 100$ (eq. 19) in the range required to explain the most luminous FRB sources (Fig. 2). As the merger proceeds and the accretion rate rises exponentially, the nature of the gaseous environment surrounding the binary is likely to becoming increasingly "messy", eventually leading to a cessation of FRB activity, at the very latest once the compact object plunges into the donor star or is completely engulfed by the common envelope on the timescale $\sim \tau_{\rm unst}$.

If a system undergoing unstable accretion were to generate multiple FRBs, the "runaway" process could impart a systematic variation in the FRB properties approaching the dynamical plunge. For example, as the accretion rate rises exponentially—and the beaming fraction presumably shrinks—one might expect the isotropic luminosity of the bursts to increase in time, at least initially. It would also be expected that the averages of other FRB properties (e.g. radio frequency) could undergo secular evolution approaching the merger, though we do not attempt to make detailed predictions for these changes here.

3.2. *Source Rates*

Assuming that all FRB are repeaters with a luminosity function similar to FRB121102, Nicholl et al. (2017) place a constraint on the volumetric space density of FRB sources, $\mathcal{N}_{\rm FRB}$ (see also Lu & Kumar 2016). The latter can expressed as the product of the FRB source formation rate $\mathcal{R}$ and the average active lifetime τ, viz.

$$\mathcal{N}_{\rm FRB} = \mathcal{R} \cdot \tau \sim 1.3 \times 10^4 \left(\frac{f_{\rm b}}{0.1}\right)^{-1} \left(\frac{\zeta}{0.1}\right)^{-1} {\rm Gpc}^{-3}, \qquad (23)$$

where $f_{\rm b}$ and ζ are the average beaming fraction and duty cycle, respectively (which may be related by the common geometry of the accretion funnel; Section 3.3).

One relevant comparison is to the volumetric rate of ULX sources. The local rate of all ULX (defined by X-ray luminosities $L_{\rm X} > 10^{39}$ erg s^{-1}) is $\mathcal{N}_{\rm ULX,39} \sim 2 \times 10^7$ Gpc^{-3} (Swartz et al. 2011). However, the luminosity function decreases moving to the higher luminosities required in our scenario to power FRBs, exhibiting a sharp break above $L_{\rm X} \sim 10^{40}$ erg s^{-1} (Mineo et al. 2012), such that the rate above $L_{\rm X} \sim 10^{41}$ erg s^{-1} is $\mathcal{N}_{\rm ULX,41} \sim 10^4$ Gpc^{-3}. Yet more luminous ULX with $L_{\rm X} \gtrsim 10^{42}$ erg s^{-1}, such as the "hyper-luminous" source HLX-1 (Farrell et al. 2009), are even less common (Gao et al. 2003).

For stable-accreting systems the maximum FRB active lifetime is of the order of the Kelvin-Helmholtz time, $\tau_{\rm KH}$ (eq. 16). Accounting for the bulk of the FRB population through this channel ($\tau = \tau_{\rm KH}$ in eq. 23) then requires a source formation rate

$$\mathcal{R}_{\rm stable} \sim 0.02 \left(\frac{m_\star}{10}\right)^{1.6} \left(\frac{f_{\rm b}}{0.1}\right)^{-1} \left(\frac{\zeta}{0.1}\right)^{-1} {\rm Gpc}^{-3} {\rm yr}^{-1}. \qquad (24)$$

Based on modeling of stable thermal mass-transfer systems, Pavlovskii et al. (2017) estimate a Milky Way formation rate of $\sim 3 \times 10^{-5}$ yr^{-1} binaries with mass-transfer rates $\dot{M}_{\rm tr} \gtrsim 100 \dot{M}_{\rm Edd}$, corresponding roughly to $\mathcal{R} \sim 100$ Gpc^{-3} yr^{-1}. The rate is higher in sub-solar metallicity environments (Section 4.1). Thus, only a small fraction $\lesssim 10^{-3}$ of potentially stable super-Eddington systems need serve as active FRB sources. This suggests an extra variable would need to be responsible for making a small fraction of ULX binaries into FRB sources.

As discussed in Section 2.5, several special conditions may indeed need to be met to produce an observable FRB. For example, generating a flare of sufficient power may require a large magnetic flux threading the BH, a task aided if the mass-transferring star is itself highly magnetized. Although strongly magnetized massive stars are relatively common (e.g., the magnetic A-stars, with a 10% occurrence rate), very few magnetic stars are in binaries (see Shultz et al. 2015 for an exception). This low binary fraction could be explained if strong magnetic fields are the result of stellar mergers (e.g. Schneider et al. 2019). In such a case, forming a mass-transferring binary with a magnetized secondary might require a low-probability scenario, such as chaotic evolution or Kozai-Lidov oscillations in an initial hierarchical triple or quadrupole system (which acts to bring a magnetized stellar merger product into contact with the NS/BH primary).

As discussed earlier, powering the most luminous FRB sources may require the very high accretion rates achieved by systems undergoing unstable mass transfer just prior to undergoing a merger or entering a common envelope phase. Applying the shorter lifetime of unstable systems, $\tau_{\mathrm{unst}} \ll \tau_{\mathrm{KH}}$ (eq. 22) to equation (23), leads to a higher required rate of unstable events:

$$\mathcal{R}_{\mathrm{unst}} \sim 5 \times 10^3 \left(\frac{f_{\mathrm{unst}}}{0.1} \right) \left(\frac{\tau_{\mathrm{unst}}}{100 P_{\mathrm{orb}}} \right)^{-1} \left(\frac{P_{\mathrm{orb}}}{10\,\mathrm{d}} \right)^{-1}$$
$$\times \left(\frac{f_{\mathrm{b}}}{0.01} \right)^{-1} \left(\frac{\zeta}{0.1} \right)^{-1} \mathrm{Gpc}^{-3}\,\mathrm{yr}^{-1}, \qquad (25)$$

where f_{unst} is the fraction of the FRB population arising from unstably accreting systems and we have scaled f_{b} to a smaller value as expected for $\dot{m} \gg 10$ (eq. 4).

The rate (25) is usefully compared to that of luminous red novae (LRN) transients, optical transients which result from stellar mergers (Soker & Tylenda 2006; Tylenda et al. 2011). For the most luminous LRN, which are thought to arise from the merger of relatively massive stars $\gtrsim 10 M_{\odot}$, Kochanek et al. (2014) estimate a rate of $\mathcal{R}_{\mathrm{LRN}} \sim 10^5\,\mathrm{Gpc}^{-3}\,\mathrm{yr}^{-1}$. Although the merging systems harboring BH/NS primaries of interest here will be rarer than ordinary massive stellar mergers, the rates (within the uncertainties) may be consistent with the most luminous FRBs arising from unstable binaries.

3.3. Periodicity

The bursts from FRB 180916 and 121102 arrive in a consistent phase window associated with a period of $\approx 16.35 \pm 0.15$ d and 161 ± 5 d, respectively (Chime/Frb Collaboration et al. 2020; Rajwade et al. 2020; Cruces et al. 2021). In previous scenarios attributing FRBs to NS activity in a binary, this periodicity was proposed to result from free-free absorption by the companion star wind (e.g., Lyutikov et al. 2020). However, such a scenario predicts a narrower observing window at lower radio frequencies, in tension with observations of FRB 180916 (Pastor-Marazuela et al. 2020; Pleunis et al. 2020). By contrast, in the super-Eddington accretion scenario presented here, a more natural explanation arises from geometric beaming by the narrow clean funnel as the BH jet crosses the observer line of sight (Fig. 1; see also Katz 2017).

Two timescales naturally arise in association with a binary, that of orbital motion and that due to disk/jet precession. An orbital period could in principle manifest in the window of FRB activity in the case of a mildly eccentric binary in which mass transfer is maximal during pericenter passage. For a semi-detached binary of mass ratio $q \equiv M_{\star}/M_{\bullet}$, the orbital period is related to the mean density of the mass-transferring star $\bar{\rho}_{\star}$ according
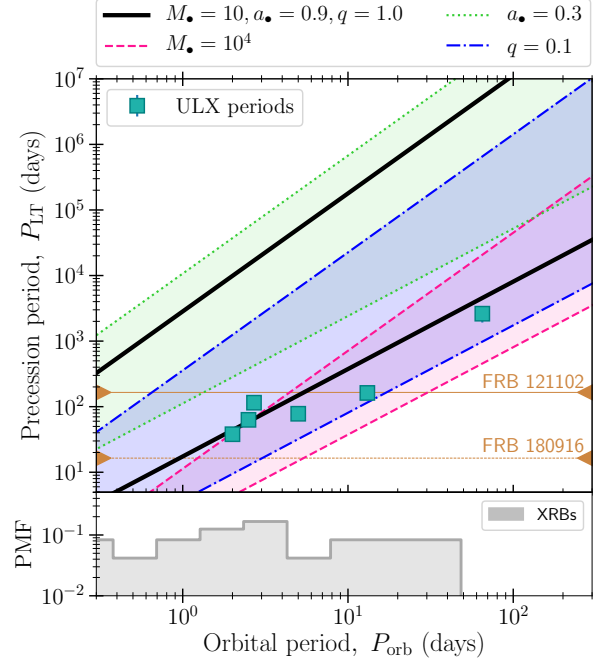
Figure 4: *Top panel:* The relationship between the BH-companion star orbital period (P_{orb}) and the Lens-Thirring precession period (P_{LT}) of inner thick accretion disk. The band covered between the solid black lines represent the range of P_{LT} values for a fiducial case: $M_{\bullet} = 10 M_{\odot}, a_{\bullet} = 0.9, q = 1.0$. The upper and lower limits of $P_{\mathrm{LT}}(P_{\mathrm{orb}})$ are set by the nature of the disk outflow—RIAF-like and negligible outflows—parametrized by $p = 0.7$ and $p = 0$, respectively (see eqs. 18 and 30). The region covered between the green (dotted), blue (dash-dotted), and pink (dashed) bands each denote the independent variation of $a_{\bullet} (= 0.3)$, $q (= 0.1)$, and $M_{\bullet} (= 10^4 M_{\odot})$, respectively, from the fiducial case. The observed ~ 160 days periodicity in FRB 121102 and the ~ 16 days periodicity in FRB 180916—corresponding to P_{LT} in the paradigm presented here—are denoted by brown horizontal lines connecting the left and right facing triangles. The green squares denote the periodicities observed in ULXs, where we interpret the observed super-orbital periods as P_{LT}. The represented ULXs are: NGC 7793 P13 (Motch et al. 2014), SS 433 (Abell & Margon 1979), M82 X-2 (Bachetti et al. 2014; Brightman et al. 2019), M51 ULX-7 (Rodríguez Castillo et al. 2020; Brightman et al. 2020), NGC 5907 ULX-1 (Walton et al. 2016; Israel et al. 2017), NGC 5408 X-1 (Grisé et al. 2013). *Bottom panel:* The probability mass function of orbital periods of bright Galactic X-ray Binaries ($L_{\mathrm{X}} > 10^{38}\,\mathrm{erg\,s^{-1}}$; grey) obtained from the WATCH-DOG catalog (Tetarenko et al. 2016).

to (Paczyński 1971)

$$P_{\rm orb} \simeq 0.35\,{\rm d} \left(\frac{2}{1+q}\right)^{0.2} \left(\frac{\bar{\rho}_\star}{\bar{\rho}_\odot}\right)^{-1/2}$$

$$\underset{q\sim1}{\approx} 0.88\,{\rm d} \left(\frac{m_\star}{10}\right)^{0.4} \left(\frac{R_\star}{R_\star^{\rm MS}}\right)^{3/2}, \qquad (26)$$

where in the final line we have scaled the stellar radius $R_\star$ to its main sequence value ($r_\star \propto m_\star^{0.6}$; $\bar{\rho}_\star \approx m_\star/r_\star^3 \approx m_\star^{-0.8}$). To reach the observed periods of tens or hundreds of days, the companion star would need to be significantly evolved off the main sequence, consistent with the mass-transfer scenarios outlined in Section 3.1, for which $R_\star \sim (1-100)R_\star^{\rm MS}$ (Pavlovskii et al. 2017).

Another potential source of periodicity can arise due to precession of the accretion funnel along which the FRB is beamed (Section 2.3). If the spin axis of the accreting BH or NS is misaligned with the angular momentum axis of the disk, then the Lens-Thirring (LT) torque applied by the rotating spacetime on the disk may cause the latter to precess (e.g., Middleton et al. 2019). Numerical simulations have shown that for thick disks (with vertical aspect ratio $h/r \gtrsim 0.05$ and low effective α viscosity), the warp propagation timescale is shorter than the differential precession timescale, thereby allowing them to precess as rigid bodies with negligible warping (Fragner & Nelson 2010). The LT precession time in this case is roughly given by (e.g. Fragile et al. 2007; Stone & Loeb 2012)

$$P_{\rm LT} \approx \frac{\pi G M_\bullet}{c^3} \frac{(1+2\xi)}{(5-2\xi)} \frac{R_{\rm out}^{5/2-\xi} R_{\rm in}^{1/2+\xi}}{R_{\rm g}^3 a_\bullet}, \qquad (27)$$

where $a_\bullet$ is the dimensionless BH spin, and $\Sigma \propto r^{-\xi}$ the surface density of the disk extending from the inner radius $R_{\rm in} \sim R_{\rm isco}$[6] to an outer radius $R_{\rm out} \gg R_{\rm isco}$. For RIAFs, $\Sigma \propto r^{p-1/2}$ (e.g. Blandford & Begelman 1999), such that for $p = 0.7$ we have $\xi = -0.2$. On the other hand, $p = 0$ (i.e. $\xi = 0.5$) when all the mass transferred from the companion star reaches the BH ($\dot{M}_{\rm tr} = \dot{M}_\bullet$; see 18). The precise load of the outflow is uncertain ($0 < p < 0.7$), and considering its limits, equation (27) becomes

---

[6] Recent works by Sridhar et al. (2019, 2020); Connors et al. (2020); Connors et al. (2021) have tracked the inner accretion flow properties of microquasars across the bright, ballistic jet-emitting states during an X-ray outburst with state-of-the-art X-ray reflection models, and have demonstrated that the inner edge of the accretion disk extends to $R_{\rm in} \sim R_{\rm isco}$ at these states.

$$P_{\rm LT} \approx \begin{cases} \frac{\pi}{9a_\bullet} \frac{R_{\rm g}}{c} \left(\frac{R_{\rm out}}{R_{\rm g}}\right)^{2.7} \left(\frac{R_{\rm isco}}{R_{\rm g}}\right)^{0.3}, & p = 0.7 \\ \frac{7\pi}{8a_\bullet} \frac{R_{\rm g}}{c} \left(\frac{R_{\rm out}}{R_{\rm g}}\right)^2 \left(\frac{R_{\rm isco}}{R_{\rm g}}\right), & p = 0.0 \end{cases} \qquad (28)$$

Taking the outer edge of the disk $R_{\rm out} \approx R_{\rm RLOF}/3$ close to the circularization radius (Frank et al. 2002), where (for $0.1 \lesssim q \lesssim 0.8$) we have (Paczyński 1971)

$$\frac{R_{\rm RLOF}}{a} \simeq 0.462 \left(\frac{q}{1+q}\right)^{1/3}, \qquad (29)$$

and a is the binary semi-major axis. Using Kepler's second law, $P_{\rm orb} = 2\pi \left[a^3/GM_\bullet(1+q)\right]^{1/2}$, equation (28) becomes

$$P_{\rm LT} \approx \begin{cases} 2.8 \times 10^3\,{\rm d} \frac{(q_{1.0}P_{\rm orb,d}^2)^{0.9}}{a_{\bullet,0.9}(m_\bullet/10)^{0.8}}, & p = 0.7 \\ 17\,{\rm d} \frac{(q_{1.0}P_{\rm orb,d}^2)^{2/3}}{a_{\bullet,0.9}(m_\bullet/10)^{1/3}}, & p = 0.0 \end{cases} \qquad (30)$$

Depending on the BH spin, mass, and mass ratios, precession timescales of tens to thousands of days are possible even from binaries with orbital periods of days (Fig. 4). A similar model was proposed to explain the 164 d jet precession timescale of SS433 (Sarazin et al. 1980; Katz 1981). Superorbital periods in the range of tens to a hundred days, which could be attributed to precession, have been observed in several ULX with sufficient X-ray coverage (e.g., Grisé et al. 2013; Brightman et al. 2019, 2020; Vasilopoulos et al. 2020; see Weng & Feng 2018 for a systematic search with *Swift*).

In FRB 180916 the observed activity window is narrower, and peaks earlier in phase, at higher radio frequencies (Pastor-Marazuela et al. 2020). Furthermore, the low-frequency bursts are observed exhibit greater average fluences (Pastor-Marazuela et al. 2020; Pleunis et al. 2020). In the synchrotron maser scenario (Section 2.5), the peak frequency of the radio emission scales with the properties of the FRB-generating transient flare and the pre-existing quiescent jet, as (eq. 14)

$$\nu_{\rm pk} \propto \frac{L_{\rm q}^{3/4}}{\Gamma_{\rm q}^2 L_{\rm f}^{1/4}} \qquad (31)$$

Thus, if the quiescent jet is "structured" in angle θ measured relative to the jet axis, with both $L_{\rm q}$ and $\Gamma_{\rm q}$ growing towards the jet edge, then lower frequency bursts would be preferentially observed at phases near the edges of the observing window (see Figs. 1 and 5). Motivating such a structure, MHD simulations of relativistic magnetized jets find that the jet Poynting flux is concentrated in a hollow cone around the jet core (e.g., Tchekhovskoy et al. 2008). In addition, since the efficiency of the synchrotron maser emission depends on
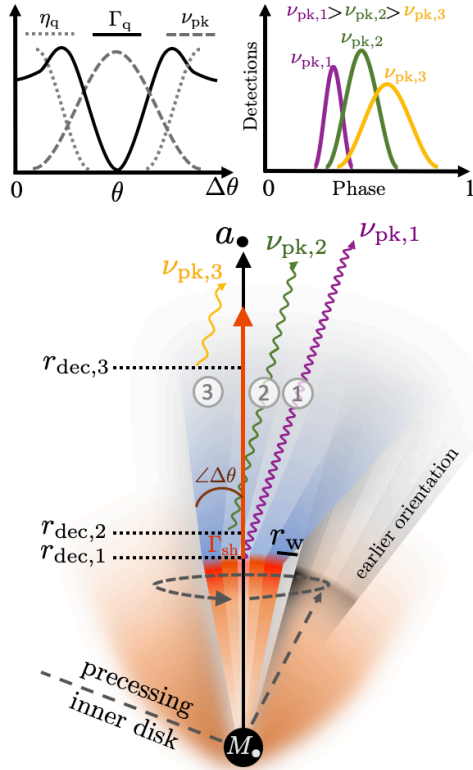
Figure 5: A curved quiescent jet cavity (blue bands) is bent towards its earlier orientation (grey cone) due to the drag of the precessing disk winds (brown) at a scale of $r_{\rm w}$ (eq. 33). The FRB-emitting flaring ejecta (red bands) are launched along the instantaneous jet axis (red vertical line with arrow), which propagates into an asymmetric (spirally curved) upstream medium. The frequency of the burst depends on whether the flare interacts with the core or sheath of the quiescent jet. The varying properties of the quiescent jet ($\Gamma_{\rm q}$ and $\eta_{\rm q}$; e.g., Tchekhovskoy et al. 2008), and the resulting synchrotron maser's peak frequency $\nu_{\rm pk}$ (eq. 31) as a function of angle θ from the jet axis are represented by the schematic at the top-left corner. The larger interaction region of the flare with the sheath of the jet implies that the observed phase window of the low-frequency bursts are wider than the higher frequency bursts. The shock deceleration radius $r_{\rm dec}$ is shorter for flares interacting with the spine of the jet compared to the interaction produced near the sheath. This implies that the high-frequency bursts lead the lower frequency ones, and are shorter in burst widths than the lower frequency ones ($t_{\rm FRB} \sim r_{\rm FRB}/(2\Gamma^2 c)$; Metzger et al. 2019). This frequency-dependent phase-window, and arrival times of bursts are shown by dividing the jet into three regions, and the corresponding detection phase-windows (arbitrary normalization) are represented in the schematic at the top-right corner.

the magnetization of the upstream medium (Plotnikov & Sironi 2019), angular structure in the magnetization of the quiescent jet could also imprint systematic variations in the luminosity of the bursts across the observing window (and hence with radio frequency; see Fig. 1).

As far as the lag in the central phase of FRB activity with radio frequency (Pastor-Marazuela et al. 2020), we speculate that it could result from the curvature of quiescent jet cavity due to the effect of precession-driven motion on the disk winds (see Section 4.2). Even if the FRB-emitting flare ejecta is launched ballistically outwards along the axis defined by the instantaneous base of the jet, by the radii of emission $\gtrsim r_{\rm dec} \sim 10^{14}$ cm (eq. 12) the medium into which the shock propagates could exhibit asymmetry between the leading and trailing edges of the precession cone, as the wind shaping the jet cavity walls is dragged back against the direction of precession. This possibility and how it relates to the angular structure of the jet discussed above, is illustrated schematically in Figure 5.

Alternatively, some low-frequency FRBs could be intrinsically higher-frequency bursts viewed slightly off-axis from the direction of the emitting shock front (such that the observed emission is Doppler-shifted to lower frequency). In this situation, the peak frequency in the observer frame will decrease, and the burst duration increase, both by the same factor (Beniamini & Kumar 2020), i.e. $\nu_{\rm off}/\nu_{\rm on} = t_{\rm off}/t_{\rm on}$ (where the subscript off / on corresponds to observed quantities for an observer who is off / on-axis to the direction along the outflow's velocity). If the relativistic outflow is directed across a narrow range of angles along the core of the jet, this could potentially result in a wider phase window for the low-frequency off-axis bursts.

4. ADDITIONAL PREDICTIONS

4.1. *Host Galaxies and Environment*

Based on HST imaging of 8 FRB host galaxies with sub-arcsecond localization, Mannings et al. (2020) find that FRBs reside in fainter regions in terms of their IR light (consistent with the locations of core collapse supernovae but not of the most massive stars; see also Bhandari et al. 2020; Heintz et al. 2020; Li & Zhang 2020). Tendulkar et al. (2020) likewise rule out significant star formation or an HII region at the location of FRB 180916; their upper limits on the $H\alpha$ luminosity at the burst location constrain potential stellar companions to be cooler than the spectral type O6V. Given the spatial offset of FRB 180916 from the nearest young stellar clump, Tendulkar et al. (2020) further argue for a source age $\gtrsim 0.8 - 7$ Myr given the expected range of projected velocities of pulsars, magnetars, or neutron stars in bina-
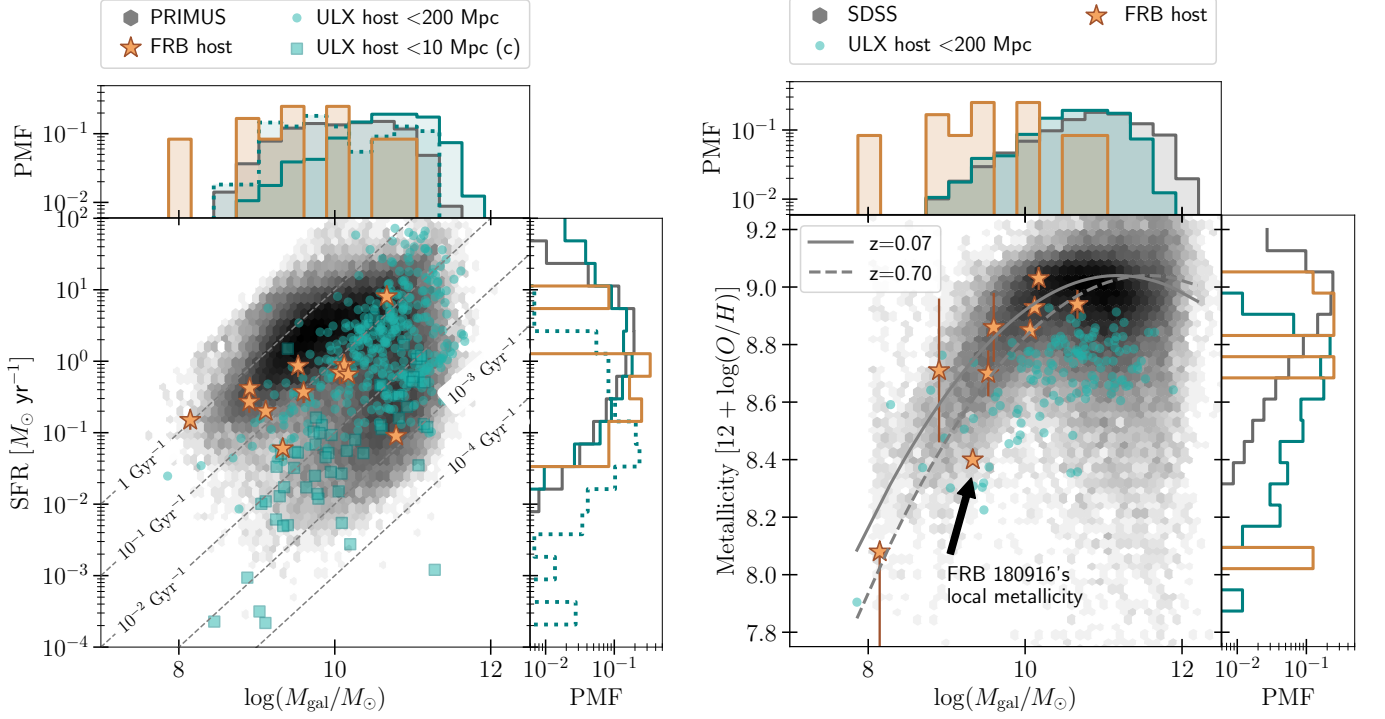
Figure 6: *Left panel:* Stellar mass and the star formation rate of the host galaxies of ULXs (green circles, and squares, from the large ($\lesssim$200 Mpc) but incomplete HECATE sample of Kovlakas et al. 2020, and the smaller ($\lesssim$ 10 Mpc) but complete Swartz et al. 2011 sample) and FRBs (brown stars; Heintz et al. 2020), in comparison to a sample of field galaxies from the PRIMUS catalog (grey; Coil et al. 2011). The top and right panels denote the probability mass functions (PMF) of $\log(M_{\rm gal}/M_\odot)$ and SFR, respectively; dark grey and brown colors represent the PRIMUS sample and FRB hosts, and the dotted and solid green histograms correspond to the ULX hosts from large/incomplete and small/complete samples, respectively. Grey dashed lines denote contours of specific SFR. *Right panel:* Stellar mass and the metallicity of the host galaxies of ULXs (Kovlakas et al. 2020) and FRBs (Heintz et al. 2020, and references therein) in comparison to a sample of SDSS emission line star-forming galaxy sample (grey; e.g., Fig. 9 of Heintz et al. 2020). The solid and dashed grey curves denote the empirical mass-metallicity relations (Maiolino et al. 2008) for redshifts $z = 0.07$ and and $z = 0.7$, respetively. The local ($\lesssim$60 pc) metallicity of FRB 180916 (Tendulkar et al. 2020) is also marked for comparison. The top and right panels denote the PMF of $\log(M_{\rm gal}/M_\odot)$ and $12 + \log(O/H)$, respectively; dark grey, green and brown colors represent the SDSS sample, ULX hosts and FRB hosts, respectively.

ries. These observations are consistent with the scenario described thus far in which FRBs arise from binaries undergoing mass-transfer from a companion star following its main sequence lifetime, which is $\sim 20(10)$ Myr for a $10(20)M_\odot$ star (e.g., Zapartas et al. 2017).

Poutanen et al. (2013) find a spatial correlation in the Antennae galaxies between the ULX sources and young stellar clusters (< 6 Myr). Furthermore, they show that most ULXs are displaced outside of the clusters, suggesting the massive ULX binaries were ejected out of the star clusters—likely due to strong gravitational encounters. FRBs also show evidence for offsets from regions of intense star formation (Tendulkar et al. 2020; Mannings et al. 2020) and have in at least one case been localized

to a region between two potentially interacting galaxies (Law et al. 2020), perhaps akin to a more distant version of the Antennae.

If FRBs arise from mass-transferring binaries similar to ULX sources, then they might be expected to occupy similar host galaxies and locations within their hosts. The left panel of Figure 6 shows the star formation rate (SFR) and stellar mass ($M_{\rm gal}$) of FRB hosts from Heintz et al. (2020) compared to those of luminous ULX. The hosts of FRBs and ULXs are generally forming stars at lower rates than the normal galaxies at a given stellar mass (e.g., below the main sequence of the star formation galaxies, or the locus with a higher specific SFR of ~ 1 Gyr^{-1}; see also Heintz et al. 2020). While the hosts
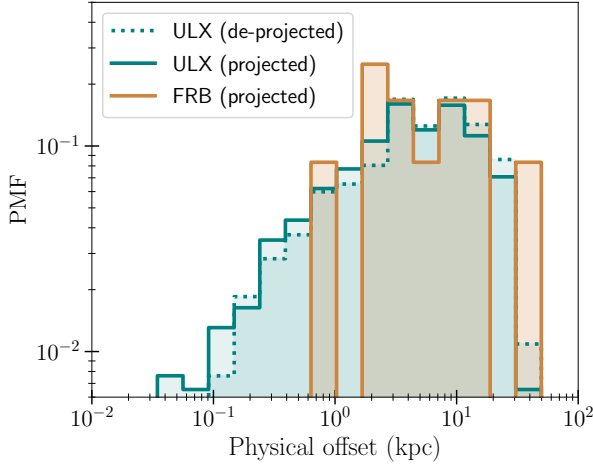
Figure 7: The probability mass function (PMF) of the projected physical offsets (in kpc) of ULX and FRB sources from their respective host galactic centers are represented by the solid green and brown histograms. The dotted green histogram corresponds to the de-projected offsets of ULX, for comparison. FRB offsets are obtained from Heintz et al. (2020), and ULX offsets are calculated from the HECATE catalog (Kovlakas et al. 2020), and the references therein.

of some FRBs and ULXs are also in the quiescent cloud (e.g., Swartz et al. 2011; Walton et al. 2011; Ravi 2019), they both occur at a greater frequency in hosts with SFR $> 0.1\,M_\odot\,\mathrm{yr}^{-1}$, as seen in the field galaxy population. James et al. (2021) found that the FRB rate, $\Phi(z) \propto (\mathrm{SFR}(z)/\mathrm{SFR}(z=0))^n$ evolves with SFR relative to the cosmological average $\mathrm{SFR}(z)$ with a power law index $n = 1.36^{+0.25}_{-0.51}$. This is consistent with the SFR-evolution of ULX population, for which $n = 0.91^{+0.10}_{-0.15}$ (Mapelli et al. 2010).

The FRB hosts are seen to be systematically less massive than those in our ULX sample. As emphasized by Bochenek et al. (2020b), comparing FRB host galaxies (typical redshift $z \sim 0.1 - 1$) to nearby galaxy populations such as our ULX sample ($\lesssim 200$ Mpc) can be problematic due to the cosmological evolution effects, particularly the shift in star-formation to lower mass galaxies with decreasing redshift. If FRBs indeed trace star formation, this could further exacerbate the tension between ULX and FRB host galaxy masses. On the other hand, the ULX sample we have used is not com-
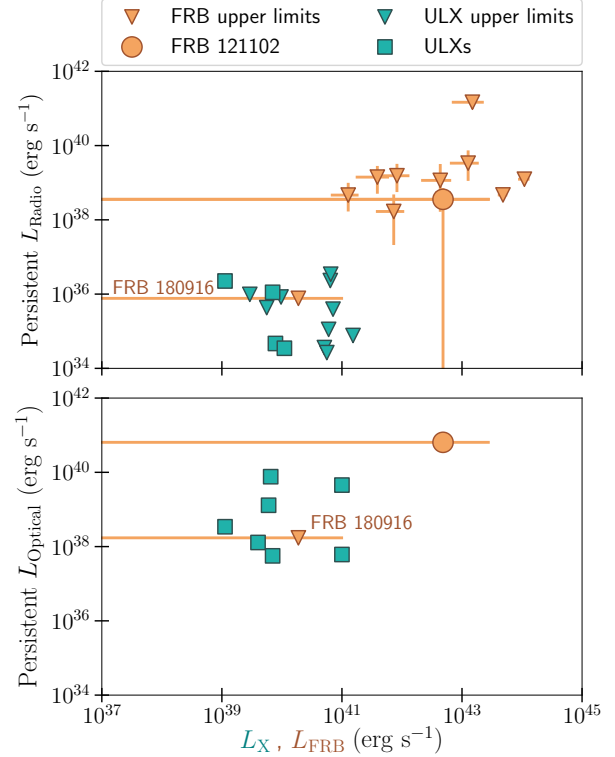
Figure 8: Luminosities of the persistent radio (upper panel) and optical (lower panel) counterparts to FRBs (brown) and ULXs (green) against their respective radio burst or X-ray luminosities (horizontal axis). Detections and upper limits are shown with squares and upside down triangles, respectively. Persistent radio counterparts and the X-ray luminosities of the represented ULXs are obtained from Kaaret et al. (2003), Miller et al. (2005), Roberts et al. (2006), Mezcua et al. (2013a,b), Sutton et al. (2013a,b), Luangtip et al. (2016), and Earnshaw et al. (2019). The persistent radio luminosity from FRBs are obtained from Yang et al. (2020) and the references therein. Luminosity of the ULX persistent optical counterparts are calculated from the reported optical magnitudes for Holmberg IX X-1, NGC 5204 X-1 (Pakull & Mirioni 2002), Holmberg II X-1 (Lehmann et al. 2005), HLX-1 (Soria et al. 2010), NGC 6946 (Kaaret et al. 2010), NGC 4559 X-10, and NGC 4395 ULX-1 (Vinokurov et al. 2018). The luminosity of the persistent optical counterparts to FRB 121102 and 180916 are calculated from the optical magnitudes reported in Chatterjee et al. (2017) and Tendulkar et al. (2020), respectively.

plete and hence is biased in the other direction, against low mass galaxies.[7]

The right panel of Figure 6 compares the metallicities of the FRB and ULX hosts in our sample. The first repeating source, FRB 121102, took place in a low metallicity dwarf galaxy (Tendulkar et al. 2017). However, there is now firm evidence from a larger sample of host galaxy properties and spatial offsets that the FRB population does not exhibit as strong of a preference for low metallicity as long duration GRBs or superluminous supernovae (Bhandari et al. 2020; Li & Zhang 2020; Mannings et al. 2020).

ULX exhibit a clear preference for lower metallicities (e.g., Walton et al. 2011; Prestwich et al. 2013), which theoretically has been attributed to the prevalence of more massive BHs at low metallicity (e.g., Mapelli et al. 2010) and other binary evolutionary effects (e.g. Pavlovskii et al. 2017; Marchant et al. 2017). Figure 6 shows that the ULX population extends to lower metallicities than the ULX hosts. On the other hand, at the location of FRB 180916, Tendulkar et al. (2020) find a low metallicity of $12 + \log(O/H) \simeq 8.4$ corresponding to $Z \approx Z_\odot/2$. Furthermore, the observed ULX population could be biased towards long-lived binary systems, while FRB sources may conversely be produced by binary systems undergoing unstable mass transfer (i.e., those which reach the highest accretion rates; Section 3.2). Systems undergoing unstable mass-transfer systems may preferentially occur at higher metallicity, e.g. due to the dependence of the stability criterion on the mass of the primary BH. A fraction of ULX may also arise from intermediate mass black holes (IMBH; Miller & Colbert 2004), which are potentially too massive to generate the shortest FRBs (Fig. 2).

The projected physical offsets of FRB sources (Heintz et al. 2020) and ULXs (Kovlakas et al. 2020) from their respective host galaxy centers are represented in Figure 7. The two offset distributions broadly overlap at large offsets, but FRBs exhibit a deficit of short offset sources relative to the ULX population.[8] This difference may not be intrinsic. The detection of FRB sources with

small offsets may be biased against, due to the decreasing FRB detection closer to the host center arising from increased DM scattering (e.g., Heintz et al. 2020).

4.2. Local Environment and Nebular Emission

One of the hallmarks of super-Eddington accretion flows are powerful, mass-loaded outflows (e.g., Blandford & Begelman 1999; King et al. 2001). There is direct evidence in ULX systems for winds with super-Eddington mechanical powers (Soria et al. 2014) carrying a total energy $\sim 10^{52}$ erg (Roberts et al. 2003), which can exceed the radiative output by up to a factor of a thousand (Pakull et al. 2010).

The mass-loss rate in super-Eddington winds $\dot{M}_w$ is expected to be comparable to the binary mass transfer rate $\dot{M}_{\rm tr}$ (eq. 15). The density profile of such an outflow of velocity $v_{\rm w}$, at radii much larger than the binary separation, can be approximated as

$$ n_w \simeq \frac{\dot{M}_w}{4\pi v_w m_p r^2}. \qquad (32) $$

If the accretion disk is undergoing precession with a period P (Fig. 1), then any ballistic ejection of material along the instantaneous jet direction will encounter the disk wind material from an earlier orientation of the disks by a radial scale no larger than:

$$ r_{\rm w} \sim P\zeta v_w \approx 7.5 \times 10^{15} {\rm cm} \left(\frac{\zeta}{0.3}\right) \left(\frac{P}{100\,{\rm d}}\right) \left(\frac{v_w}{0.1c}\right). \qquad (33) $$

The Thomson column of this material encountered by an FRB emitted at smaller radii can be estimated as

$$ \tau_{\rm T,w} \simeq n_w(r_w)\sigma_{\rm T} r_{\rm w} \approx \frac{\dot{M}_w \sigma_{\rm T}}{4\pi m_p v_w r_{\rm w}} $$
$$ \sim 1.8 \times 10^{-9} \left(\frac{\dot{M}_w}{\dot{M}_{\rm Edd}}\right) \left(\frac{m_\bullet}{10}\right) \left(\frac{r_{\rm w}}{10^{16}{\rm cm}}\right)^{-1} \left(\frac{v_{\rm w}}{0.1\,c}\right)^{-1}. \qquad (34) $$

For $\dot{M}_{\rm w} \gg \dot{M}_{\rm Edd}$, time variability of this column could generate variations in $DM \approx 5 \times 10^5 \tau_{\rm T}$ over the timescale P, distinct from that accumulated through the quiescent jet cavity (eq. 10). If the accretion disk wind is magnetized, then propagation through it could generate a more significant local time-variable rotation measure (RM) across the active phase (see inset of Fig. 1), as observed in FRB 180916 (Pleunis et al. 2020) and FRB 121102 (Hessels et al. 2019; although the latter could originate from a wind-fed nebula on larger scales; Margalit & Metzger 2018). As with the DM above, we estimate the RM contribution through the precessing disk

---

[7] An exact comparison between the HECATE ULX galaxies and the PRIMUS galaxy sample is also complicated by the different indicators (spectral bands) used to determine their respective SFRs. For example, infrared-based SFR indicators are most reliable for late-type galaxies.

[8] The ULX sources from the HECATE sample (Kovlakas et al. 2020) are drawn only from within the D25 region of the host galaxy (i.e., the radius of the isophote where the observed band's surface brightness is 25 mag arcsec^{-2}). Therefore, the spatial distribution of the ULXs within their hosts are limited by the radius of the selection region, and is devoid of sources with larger offsets belonging to an exponentially decreasing tail of the distribution.

wind (at radii $\gtrsim r_{\rm w}$) to be

$$\text{RM} \sim \frac{e^3}{2\pi m_e^2 c^4} B_{\rm w} n_{\rm w}(r_{\rm w}) r_{\rm w} \sin\alpha \approx 0.5\,\text{rad}\,\text{m}^{-2}\left(\frac{\sin\alpha}{0.1}\right) \times$$

$$\left(\frac{\sigma_{\rm w}}{0.01}\right)^{1/2}\left(\frac{\dot{M}_w}{\dot{M}_{\rm Edd}}\right)^{3/2}\left(\frac{m_\bullet}{10}\right)^{3/2}\left(\frac{v_{\rm w}}{0.1\,c}\right)^{-3/2}\left(\frac{r_{\rm w}}{10^{16}{\rm cm}}\right)^{-2}\!\!(35)$$

where $\sigma_{\rm w} = B_{\rm w}^2/(4\pi n_{\rm w} m_p c^2)$ is the radially constant magnetization of the wind and α is an appropriate average angle between the directions of the magnetic field and the FRB path of propagation.

At larger radii $r \sim 10^{17}$ cm, the wind density for fiducial parameters ($\dot{M}_{\rm w} \sim 10^3 \dot{M}_{\rm Edd}$; $M_\bullet \sim 10 M_\odot$; $v_{\rm w} \lesssim 0.1c$) is $n_w \gtrsim 10$ cm^{-3}. This could provide the required plasma for self-modulation of the FRB signal described by Sobacchi et al. (2021).

On yet larger scales of up to hundreds of parsecs, ULX outflows are observed to inflate bubbles of shock-ionized plasma capable of generating persistent optical, X-ray, and radio emission (Pakull & Mirioni 2002; Wang 2002; Kaaret et al. 2003; Ramsey et al. 2006; Soria et al. 2010). The ULX jet can also power steady non-thermal synchrotron emission on smaller scales (Miller et al. 2005; Lang et al. 2007).

Figure 8 compiles detections and upper limits on the persistent radio (top panel) and optical (bottom panel) luminosities of FRBs and ULX sources. Although many ULX are detected, most of the upper limits on FRB persistent source emission are unconstraining due to their comparatively greater distances. Nevertheless, if some FRBs indeed arise from long-lived ULX sources, the closest events may eventually exhibit detectable, and potentially resolvable, persistent emission. This would not necessarily be true for the subset of FRBs arising from short-lived binaries undergoing unstable mass transfer (Section 3), if the system is not active long enough to inflate a large bubble. The compact synchrotron radio source co-located to < 0.7 pc of FRB 121102 (Chatterjee et al. 2017; Marcote et al. 2017), could arise from young ($\sim$decades old) ULX-bubble from a binary system in the process of undergoing unstable mass transfer. The total energy $\sim 10^{50}-10^{51}$ erg and mass-outflow rate $\dot{M} \sim 10^{19} - 10^{21}$ g s^{-1} needed to simultaneously explain the radio spectrum and rotation measure of the source (Margalit et al. 2018), are indeed similar to those expected for super-Eddington disk outflows.

4.3. *Multiwavelength Transient Counterparts*

Models in which FRBs are generated by magnetized shocks predict simultaneous electromagnetic emission ranging from the optical to gamma-ray bands arising from (incoherent) thermal synchrotron emission (e.g., Metzger et al. 2019; Beloborodov 2019). Though carrying more radiated energy than the FRB itself, this counterpart is challenging to detect except for the brightest FRB sources, such as those originating from Galactic magnetar flares. X-rays were observed simultaneous with the FRB-like burst from SGR 1935+2154 (e.g., Mereghetti et al. 2020), consistent with the predictions of shock synchrotron emission (Metzger et al. 2019; Margalit et al. 2020).

As discussed in Sections 3.1 and 3.2, the most luminous accretion-powered FRB sources could arise from binary systems undergoing unstable mass transfer. These systems are predicted to be short-lived, with a lifetime of peak FRB activity of $\tau_{\rm unst} \lesssim$ years to decades (eq. 22). The end state of this process is a stellar merger or common envelope event (Ivanova et al. 2013).

Stellar merger events are commonly observed in the Milky Way and nearby galaxies as optical (Soker & Tylenda 2006) and/or dusty infrared (Kasliwal et al. 2017) transients. Most such systems are believed to arise from the merger of binaries consisting of main sequence or moderately evolved stars (e.g., Tylenda et al. 2011), i.e. not containing BH or NS primaries. However, if similar transients are generated from BH/NS merger events (as suggested by numerical simulations; e.g., Law-Smith et al. 2020), then some FRB sources−particularly the most luminous ones−could be accompanied by a LRN in the months to years after "turning off" as FRB sources. In fact, FRBs could serve as unique sign posts to this special type of stellar merger event.

LRN reach peak optical luminosities in the range $\sim 10^{39} - 10^{41}$ erg s^{-1} (e.g. Pastorello et al. 2019), corresponding to visual apparent magnitudes $\gtrsim 21 - 22$, at the distance of even the nearest FRB 180916 (≈ 150 Mpc). Such transient emission would be challenging to detect with current optical time-domain facilities, but would make promising targets for future surveys like the Vera Rubin Observatory (e.g. LSST Science Collaboration et al. 2009). We accordingly recommend that a deep optical/IR follow-up campaign be targeted on previously periodic FRB sources which suddenly "turn off" with a $\lesssim$ weekly cadence to capture the brightest phases of putative LRN emission.

If the BH spiraling inwards during the common envelope phase were to accrete gas and generate a relativistic jet, these events could in principle be a source of high-energy neutrino emission (Grichener & Soker 2021). The end state of such mergers is uncertain, with possibilities ranging from an isolated compact binary with a white dwarf secondary to a quasi-spherical Thorne-Zytkow object (Thorne & Zytkow 1975).

5. PREDICTIONS AND CONCLUSIONS

We have outlined a scenario in which recurring FRBs are powered by transient flares from accreting stellar-mass BH or NS binary systems. The high required accretion rates, which must exceed the Eddington rate to explain the most luminous FRBs, drive us to consider a potential connection to ULX sources, the closest known persistent super-Eddington sources. Although we are able to draw few definitive conclusions, we have provided semi-quantitative arguments showing how such systems could in principle account for the observed durations, energetics, beaming fraction, radio frequencies, periodic behavior, rates, and host galaxy properties. Each of these issues merits a more detailed follow-up study.

We conclude by enumerating some implications and predictions of the ULX binary scenario.

- Systems with higher accretion rates generate FRBs with narrower beaming fractions if the latter are shaped by the geometry of the super-Eddington accretion flow (e.g., $f_{\rm b} \propto \dot{M}_{\bullet}^{-2}$; eq. 4). For periodic sources, this could manifest as a narrower active phase with increasing FRB luminosity. On the other hand, coupled with the potentially shorter lifetimes of high-$\dot{M}_{\bullet}$ systems, this could result in a lower probability of identifying the most luminous FRB sources as recurring in the first place.

- The properties of FRB host galaxies, and the spatial offsets of the bursting sources within these galaxies, could track those of the most luminous ULX sources (Fig. 6). However, we warn that this correspondence may not be perfect, particularly if FRBs preferentially arise from short-lived binaries undergoing unstable mass-transfer. On smaller spatial scales, some FRB sources may coincide with luminous optical line, X-ray, radio emitting regions akin to the super-bubbles observed surrounding luminous ULX (Fig. 8).

- A fraction of known ULX may emit detectable FRBs, and we encourage systematic radio monitoring of these sources. We caution that a rate comparison suggests that atypical conditions—such as a highly magnetized secondary star—may be necessary for ULX to generate the bulk of the luminous FRBs detected at cosmological distances (Section 3.2). Nevertheless, weaker radio bursts could be detected from a targeted ULX search due to their comparatively closer distances. Evidence for transient ultra-relativistic $\Gamma > 100$ outflows from these systems, would also support an FRB connection (Fig. 3).

- Periodic sources could exhibit small systematic variations in the burst DM and RM across the active phase window due to the bursts propagating through the magnetized super-Eddington disk outflows (swept into a spiral pattern intersecting the instantaneous jet axis due to precession of the disk angular momentum). If the quiescent jet is sufficiently dilute, or the disk precession period sufficiently short, the FRB-generating flare may interact with the disk wind, potentially giving rise to more complicated evolution of the polarization across the burst than in cases in which the upstream medium is the comparatively organized quiescent jet.

- The most luminous FRB sources may arise from binaries undergoing unstable mass transfer and evolving towards a merger or common envelope event. To the extent that such sources are periodic, this could lead to systematic variations in the average burst properties with time as the accretion rate rises and the environment surrounding the FRB source evolves towards the final dynamical phase. Such short-lived sources would not exhibit the large $\gtrsim$ many parsec-scale nebulae but they could generate compact radio nebulae, such as observed around FRB 121102.

  The unstable accreting sources will "turn off" as FRB emitters on a timescale of weeks to years approaching the dynamical phase of the merger. Relatively soon after this point the system will generate a luminous optical/IR transient, akin to a luminous red nova or dusty infrared transient.

- Observed FRB durations are most consistent with arising from stellar-mass compact objects. However, a similar physical model could in principle be extended to more massive, intermediate—or even super-massive—black holes. Scaling to the larger ISCO radius (minimum variability time), one would predict the existence of "slow radio bursts" with larger maximum energy and durations significantly longer than hundreds of milliseconds (see Zhang 2020b for a different physical mechanism for generating SRBs). Future work is necessary to address the sensitivity of current or future surveys to SRBs.

ACKNOWLEDGMENTS

REFERENCES

Abell, G. O., & Margon, B. 1979, Nature, 279, 701, doi: 10.1038/279701a0

Abramowicz, M. A., Czerny, B., Lasota, J. P., & Szuszkiewicz, E. 1988, ApJ, 332, 646, doi: 10.1086/166683

Astropy Collaboration, Robitaille, T. P., Tollerud, E. J., et al. 2013, A&A, 558, A33, doi: 10.1051/0004-6361/201322068

Astropy Collaboration, Price-Whelan, A. M., SipHocz, B. M., et al. 2018, aj, 156, 123, doi: 10.3847/1538-3881/aabc4f

Atapin, K. E., & Fabrika, S. N. 2016, Astronomy Letters, 42, 517, doi: 10.1134/S106377371607001X

Babul, A.-N., & Sironi, L. 2020, arXiv e-prints, arXiv:2006.03081. https://arxiv.org/abs/2006.03081

Bachetti, M., Harrison, F. A., Walton, D. J., et al. 2014, Nature, 514, 202, doi: 10.1038/nature13791

Begelman, M. C. 2014, arXiv e-prints, arXiv:1410.8132. https://arxiv.org/abs/1410.8132

Begelman, M. C., King, A. R., & Pringle, J. E. 2006, MNRAS, 370, 399, doi: 10.1111/j.1365-2966.2006.10469.x

Beloborodov, A. M. 2017, ApJL, 843, L26, doi: 10.3847/2041-8213/aa78f3

—. 2019, arXiv e-prints, arXiv:1908.07743. https://arxiv.org/abs/1908.07743

Beniamini, P., & Kumar, P. 2020, MNRAS, 498, 651, doi: 10.1093/mnras/staa2489

Beniamini, P., Wadiasingh, Z., & Metzger, B. D. 2020, MNRAS, 496, 3390, doi: 10.1093/mnras/staa1783

Bhandari, S., Sadler, E. M., Prochaska, J. X., et al. 2020, ApJL, 895, L37, doi: 10.3847/2041-8213/ab672e

Blandford, R. D., & Begelman, M. C. 1999, MNRAS, 303, L1, doi: 10.1046/j.1365-8711.1999.02358.x

Blandford, R. D., & Znajek, R. L. 1977, MNRAS, 179, 433, doi: 10.1093/mnras/179.3.433

Bochenek, C. D., Ravi, V., Belov, K. V., et al. 2020a, arXiv e-prints, arXiv:2005.10828. https://arxiv.org/abs/2005.10828

Bochenek, C. D., Ravi, V., & Dong, D. 2020b, arXiv e-prints, arXiv:2009.13030. https://arxiv.org/abs/2009.13030

Brightman, M., Harrison, F. A., Bachetti, M., et al. 2019, ApJ, 873, 115, doi: 10.3847/1538-4357/ab0215

Brightman, M., Earnshaw, H., Fürst, F., et al. 2020, ApJ, 895, 127, doi: 10.3847/1538-4357/ab7e2a

Bromberg, O., & Tchekhovskoy, A. 2016, MNRAS, 456, 1739, doi: 10.1093/mnras/stv2591

Chatterjee, S., Law, C. J., Wharton, R. S., et al. 2017, Nature, 541, 58, doi: 10.1038/nature20797

Chen, A. Y., Yuan, Y., Beloborodov, A. M., & Li, X. 2020, arXiv e-prints, arXiv:2010.15619. https://arxiv.org/abs/2010.15619

CHIME/FRB Collaboration, Andersen, B. C., Bandura, K., et al. 2019, ApJL, 885, L24, doi: 10.3847/2041-8213/ab4a80

Chime/Frb Collaboration, Amiri, M., Andersen, B. C., et al. 2020, Nature, 582, 351, doi: 10.1038/s41586-020-2398-2

Coil, A. L., Blanton, M. R., Burles, S. M., et al. 2011, ApJ, 741, 8, doi: 10.1088/0004-637X/741/1/8

Connors, R., García, J., Tomsick, J., et al. 2021

Connors, R. M. T., García, J. A., Dauser, T., et al. 2020, ApJ, 892, 47, doi: 10.3847/1538-4357/ab7afc

Cruces, M., Spitler, L. G., Scholz, P., et al. 2021, MNRAS, 500, 448, doi: 10.1093/mnras/staa3223

Day, C. K., Deller, A. T., Shannon, R. M., et al. 2020, MNRAS, 497, 3335, doi: 10.1093/mnras/staa2138

Drenkhahn, G., & Spruit, H. C. 2002, A&A, 391, 1141, doi: 10.1051/0004-6361:20020839

Earnshaw, H. P., Grefenstette, B. W., Brightman, M., et al. 2019, ApJ, 881, 38, doi: 10.3847/1538-4357/ab20cd

Fabrika, S. 2004, Astrophys. Space Phys. Res., 12, 1. https://arxiv.org/abs/astro-ph/0603390

Farrell, S. A., Webb, N. A., Barret, D., Godet, O., & Rodrigues, J. M. 2009, Nature, 460, 73, doi: 10.1038/nature08083

Fender, R., Wu, K., Johnston, H., et al. 2004, Nature, 427, 222, doi: 10.1038/nature02137

Fragile, P. C., Blaes, O. M., Anninos, P., & Salmonson, J. D. 2007, ApJ, 668, 417, doi: 10.1086/521092

Fragner, M. M., & Nelson, R. P. 2010, A&A, 511, A77, doi: 10.1051/0004-6361/200913088

Frank, J., King, A., & Raine, D. J. 2002, Accretion Power in Astrophysics: Third Edition

Gao, Y., Wang, Q. D., Appleton, P. N., & Lucas, R. A. 2003, ApJL, 596, L171, doi: 10.1086/379598

Globus, N., & Levinson, A. 2013, PhRvD, 88, 084046, doi: 10.1103/PhysRevD.88.084046

Gourdji, K., Michilli, D., Spitler, L. G., et al. 2019, ApJL, 877, L19, doi: 10.3847/2041-8213/ab1f8a

Grichener, A., & Soker, N. 2021, arXiv e-prints, arXiv:2101.05118. https://arxiv.org/abs/2101.05118

Grisé, F., Kaaret, P., Corbel, S., Cseh, D., & Feng, H. 2013, MNRAS, 433, 1023, doi: 10.1093/mnras/stt783

Heintz, K. E., Prochaska, J. X., Simha, S., et al. 2020, arXiv e-prints, arXiv:2009.10747. https://arxiv.org/abs/2009.10747

Hessels, J. W. T., Spitler, L. G., Seymour, A. D., et al. 2019, ApJL, 876, L23, doi: 10.3847/2041-8213/ab13ae

Hillwig, T. C., & Gies, D. R. 2008, ApJL, 676, L37, doi: 10.1086/587140

Israel, G. L., Belfiore, A., Stella, L., et al. 2017, Science, 355, 817, doi: 10.1126/science.aai8635

Ivanova, N., Justham, S., Chen, X., et al. 2013, A&A Rv, 21, 59, doi: 10.1007/s00159-013-0059-2

Iwamoto, M., Amano, T., Hoshino, M., & Matsumoto, Y. 2018, ApJ, 858, 93, doi: 10.3847/1538-4357/aaba7a

James, C. W., Prochaska, J. X., Macquart, J. P., et al. 2021, arXiv e-prints, arXiv:2101.07998. https://arxiv.org/abs/2101.07998

Kaaret, P., Corbel, S., Prestwich, A. H., & Zezas, A. 2003, Science, 299, 365, doi: 10.1126/science.1079610

Kaaret, P., & Feng, H. 2009, ApJ, 702, 1679, doi: 10.1088/0004-637X/702/2/1679

Kaaret, P., Feng, H., & Roberts, T. P. 2017, ARA&A, 55, 303, doi: 10.1146/annurev-astro-091916-055259

Kaaret, P., Feng, H., Wong, D. S., & Tao, L. 2010, ApJL, 714, L167, doi: 10.1088/2041-8205/714/1/L167

Kasliwal, M. M., et al. 2017, Science, 358, 1559, doi: 10.1126/science.aap9455

Katz, J. I. 1981, A&A, 95, L15

—. 2016, ApJ, 826, 226, doi: 10.3847/0004-637X/826/2/226

—. 2017, MNRAS, 471, L92, doi: 10.1093/mnrasl/slx113

Keane, E. F., Stappers, B. W., Kramer, M., & Lyne, A. G. 2012, MNRAS, 425, L71, doi: 10.1111/j.1745-3933.2012.01306.x

King, A. R. 2009, MNRAS, 393, L41, doi: 10.1111/j.1745-3933.2008.00594.x

King, A. R., & Begelman, M. C. 1999, ApJL, 519, L169, doi: 10.1086/312126

King, A. R., Davies, M. B., Ward, M. J., Fabbiano, G., & Elvis, M. 2001, ApJL, 552, L109, doi: 10.1086/320343

Kochanek, C. S., Adams, S. M., & Belczynski, K. 2014, MNRAS, 443, 1319, doi: 10.1093/mnras/stu1226

Kolb, U. 1998, MNRAS, 297, 419, doi: 10.1046/j.1365-8711.1998.01489.x

Kovlakas, K., Zezas, A., Andrews, J. J., et al. 2020, MNRAS, 498, 4790, doi: 10.1093/mnras/staa2481

Kulkarni, S. R., Ofek, E. O., Neill, J. D., Zheng, Z., & Juric, M. 2014, ApJ, 797, 70, doi: 10.1088/0004-637X/797/1/70

Kumar, P., & Bošnjak, Ž. 2020, MNRAS, 494, 2385, doi: 10.1093/mnras/staa774

Kumar, P., Lu, W., & Bhattacharya, M. 2017, MNRAS, 468, 2726, doi: 10.1093/mnras/stx665

Kumar, P., & Zhang, B. 2015, PhR, 561, 1, doi: 10.1016/j.physrep.2014.09.008

Lang, C. C., Kaaret, P., Corbel, S., & Mercer, A. 2007, ApJ, 666, 79, doi: 10.1086/519553

Law, C. J., Butler, B. J., Prochaska, J. X., et al. 2020, ApJ, 899, 161, doi: 10.3847/1538-4357/aba4ac

Law-Smith, J. A. P., Everson, R. W., Ramirez-Ruiz, E., et al. 2020, arXiv e-prints, arXiv:2011.06630. https://arxiv.org/abs/2011.06630

Lehmann, I., Becker, T., Fabrika, S., et al. 2005, A&A, 431, 847, doi: 10.1051/0004-6361:20035827

Levin, Y., Beloborodov, A. M., & Bransgrove, A. 2020, arXiv e-prints, arXiv:2002.04595. https://arxiv.org/abs/2002.04595

Li, C. K., Lin, L., Xiong, S. L., et al. 2020, arXiv e-prints, arXiv:2005.11071. https://arxiv.org/abs/2005.11071

Li, D., & Zanazzi, J. J. 2021

Li, Y., & Zhang, B. 2020, arXiv e-prints, arXiv:2005.02371. https://arxiv.org/abs/2005.02371

Lithwick, Y., & Sari, R. 2001, ApJ, 555, 540, doi: 10.1086/321455

Lorimer, D. R., Bailes, M., McLaughlin, M. A., Narkevic, D. J., & Crawford, F. 2007, Science, 318, 777, doi: 10.1126/science.1147532

LSST Science Collaboration, Abell, P. A., Allison, J., et al. 2009, arXiv e-prints, arXiv:0912.0201. https://arxiv.org/abs/0912.0201

Lu, W., & Kumar, P. 2016, MNRAS, 461, L122, doi: 10.1093/mnrasl/slw113

—. 2018, MNRAS, 477, 2470, doi: 10.1093/mnras/sty716

Lu, W., Piro, A. L., & Waxman, E. 2020, arXiv e-prints, arXiv:2003.12581. https://arxiv.org/abs/2003.12581

22

Luangtip, W., Roberts, T. P., & Done, C. 2016, MNRAS, 460, 4417, doi: 10.1093/mnras/stw1282

Luo, R., Wang, B. J., Men, Y. P., et al. 2020, Nature, 586, 693, doi: 10.1038/s41586-020-2827-2

Lyubarsky, Y. 2008, ApJ, 682, 1443, doi: 10.1086/589435

—. 2014, MNRAS, 442, L9, doi: 10.1093/mnrasl/slu046

—. 2019, MNRAS, 483, 1731, doi: 10.1093/mnras/sty3233

—. 2020, ApJ, 897, 1, doi: 10.3847/1538-4357/ab97b5

Lyutikov, M., Barkov, M. V., & Giannios, D. 2020, ApJL, 893, L39, doi: 10.3847/2041-8213/ab87a4

MacLeod, M., & Loeb, A. 2020, arXiv e-prints, arXiv:2003.01123. https://arxiv.org/abs/2003.01123

Mahlmann, J. F., Levinson, A., & Aloy, M. A. 2020, MNRAS, 494, 4203, doi: 10.1093/mnras/staa943

Maiolino, R., Nagao, T., Grazian, A., et al. 2008, A&A, 488, 463, doi: 10.1051/0004-6361:200809678

Mannings, A. G., Fong, W.-f., Simha, S., et al. 2020, arXiv e-prints, arXiv:2012.11617. https://arxiv.org/abs/2012.11617

Mapelli, M., Ripamonti, E., Zampieri, L., Colpi, M., & Bressan, A. 2010, MNRAS, 408, 234, doi: 10.1111/j.1365-2966.2010.17048.x

Marchant, P., Langer, N., Podsiadlowski, P., et al. 2017, A&A, 604, A55, doi: 10.1051/0004-6361/201630188

Marcote, B., Paragi, Z., Hessels, J. W. T., et al. 2017, ApJL, 834, L8, doi: 10.3847/2041-8213/834/2/L8

Margalit, B., Berger, E., & Metzger, B. D. 2019, ApJ, 886, 110, doi: 10.3847/1538-4357/ab4c31

Margalit, B., & Metzger, B. D. 2018, ApJL, 868, L4, doi: 10.3847/2041-8213/aaedad

Margalit, B., Metzger, B. D., Berger, E., et al. 2018, MNRAS, 481, 2407, doi: 10.1093/mnras/sty2417

Margalit, B., Metzger, B. D., & Sironi, L. 2020, MNRAS, doi: 10.1093/mnras/staa1036

Margon, B. 1984, ARA&A, 22, 507, doi: 10.1146/annurev.aa.22.090184.002451

Mereghetti, S., Savchenko, V., Ferrigno, C., et al. 2020, arXiv e-prints, arXiv:2005.06335. https://arxiv.org/abs/2005.06335

Metzger, B. D., Berger, E., & Margalit, B. 2017, ApJ, 841, 14, doi: 10.3847/1538-4357/aa633d

Metzger, B. D., Margalit, B., & Sironi, L. 2019, MNRAS, 485, 4091, doi: 10.1093/mnras/stz700

Mezcua, M., Farrell, S. A., Gladstone, J. C., & Lobanov, A. P. 2013a, MNRAS, 436, 1546, doi: 10.1093/mnras/stt1674

Mezcua, M., Roberts, T. P., Sutton, A. D., & Lobanov, A. P. 2013b, MNRAS, 436, 3128, doi: 10.1093/mnras/stt1794

Michilli, D., Seymour, A., Hessels, J. W. T., et al. 2018, Nature, 553, 182, doi: 10.1038/nature25149

Middleton, M. J., Fragile, P. C., Ingram, A., & Roberts, T. P. 2019, MNRAS, 489, 282, doi: 10.1093/mnras/stz2005

Miller, M. C., & Colbert, E. J. M. 2004, International Journal of Modern Physics D, 13, 1, doi: 10.1142/S0218271804004426

Miller, N. A., Mushotzky, R. F., & Neff, S. G. 2005, ApJL, 623, L109, doi: 10.1086/430112

Miller-Jones, J. C. A., Fender, R. P., & Nakar, E. 2006, MNRAS, 367, 1432, doi: 10.1111/j.1365-2966.2006.10092.x

Mineo, S., Gilfanov, M., & Sunyaev, R. 2012, MNRAS, 419, 2095, doi: 10.1111/j.1365-2966.2011.19862.x

Mirabel, I. F., & Rodríguez, L. F. 1994, Nature, 371, 46, doi: 10.1038/371046a0

Motch, C., Pakull, M. W., Soria, R., Grisé, F., & Pietrzyński, G. 2014, Nature, 514, 198, doi: 10.1038/nature13730

Mushtukov, A. A., Suleimanov, V. F., Tsygankov, S. S., & Poutanen, J. 2015, MNRAS, 454, 2539, doi: 10.1093/mnras/stv2087

Narayan, R., & Yi, I. 1995, ApJ, 452, 710, doi: 10.1086/176343

Nicholl, M., et al. 2017, ApJL, 848, L18, doi: 10.3847/2041-8213/aa9029

Paczyński, B. 1971, ARA&A, 9, 183, doi: 10.1146/annurev.aa.09.090171.001151

Pakull, M. W., & Mirioni, L. 2002, arXiv e-prints, astro. https://arxiv.org/abs/astro-ph/0202488

Pakull, M. W., Soria, R., & Motch, C. 2010, Nature, 466, 209, doi: 10.1038/nature09168

Parfrey, K., Giannios, D., & Beloborodov, A. M. 2015, MNRAS, 446, L61, doi: 10.1093/mnrasl/slu162

Parfrey, K., Spitkovsky, A., & Beloborodov, A. M. 2016, ApJ, 822, 33, doi: 10.3847/0004-637X/822/1/33

Parfrey, K., & Tchekhovskoy, A. 2017, ApJL, 851, L34, doi: 10.3847/2041-8213/aa9c85

Pastor-Marazuela, I., Connor, L., van Leeuwen, J., et al. 2020, arXiv e-prints, arXiv:2012.08348. https://arxiv.org/abs/2012.08348

Pastorello, A., Mason, E., Taubenberger, S., et al. 2019, A&A, 630, A75, doi: 10.1051/0004-6361/201935999

Pavlovskii, K., Ivanova, N., Belczynski, K., & Van, K. X. 2017, MNRAS, 465, 2092, doi: 10.1093/mnras/stw2786

Pejcha, O. 2014, ApJ, 788, 22, doi: 10.1088/0004-637X/788/1/22

Pejcha, O., Metzger, B. D., Tyles, J. G., & Tomida, K. 2017, ApJ, 850, 59, doi: 10.3847/1538-4357/aa95b9

Petroff, E., Barr, E. D., Jameson, A., et al. 2016, PASA, 33, e045, doi: 10.1017/pasa.2016.35

Philippov, A., Uzdensky, D. A., Spitkovsky, A., & Cerutti, B. 2019, ApJL, 876, L6, doi: 10.3847/2041-8213/ab1590

Phinney, E. S. 1982, MNRAS, 198, 1109, doi: 10.1093/mnras/198.4.1109

Platts, E., Weltman, A., Walters, A., et al. 2019, PhR, 821, 1, doi: 10.1016/j.physrep.2019.06.003

Pleunis, Z., Michilli, D., Bassa, C. G., et al. 2020, arXiv e-prints, arXiv:2012.08372. https://arxiv.org/abs/2012.08372

Plotnikov, I., & Sironi, L. 2019, MNRAS, 485, 3816, doi: 10.1093/mnras/stz640

Popov, S. B., & Postnov, K. A. 2013, arXiv e-prints, arXiv:1307.4924. https://arxiv.org/abs/1307.4924

Poutanen, J., Fabrika, S., Valeev, A. F., Sholukhova, O., & Greiner, J. 2013, MNRAS, 432, 506, doi: 10.1093/mnras/stt487

Poutanen, J., Lipunova, G., Fabrika, S., Butkevich, A. G., & Abolmasov, P. 2007, MNRAS, 377, 1187, doi: 10.1111/j.1365-2966.2007.11668.x

Prestwich, A. H., Tsantaki, M., Zezas, A., et al. 2013, ApJ, 769, 92, doi: 10.1088/0004-637X/769/2/92

Rajwade, K. M., Mickaliger, M. B., Stappers, B. W., et al. 2020, MNRAS, 495, 3551, doi: 10.1093/mnras/staa1237

Ramsey, C. J., Williams, R. M., Gruendl, R. A., et al. 2006, ApJ, 641, 241, doi: 10.1086/499070

Rappaport, S. A., Podsiadlowski, P., & Pfahl, E. 2005, MNRAS, 356, 401, doi: 10.1111/j.1365-2966.2004.08489.x

Ravi, V. 2019, Nature Astronomy, 3, 928, doi: 10.1038/s41550-019-0831-y

Ripperda, B., Porth, O., Sironi, L., & Keppens, R. 2019, MNRAS, 485, 299, doi: 10.1093/mnras/stz387

Roberts, T. P., Goad, M. R., Ward, M. J., & Warwick, R. S. 2003, MNRAS, 342, 709, doi: 10.1046/j.1365-8711.2003.06593.x

Roberts, T. P., Kilgard, R. E., Warwick, R. S., Goad, M. R., & Ward, M. J. 2006, MNRAS, 371, 1877, doi: 10.1111/j.1365-2966.2006.10821.x

Rodríguez Castillo, G. A., Israel, G. L., Belfiore, A., et al. 2020, ApJ, 895, 60, doi: 10.3847/1538-4357/ab8a44

Safarzadeh, M., Prochaska, J. X., Heintz, K. E., & Fong, W.-f. 2020, arXiv e-prints, arXiv:2009.11735. https://arxiv.org/abs/2009.11735

Sarazin, C. L., Begelman, M. C., & Hatchett, S. P. 1980, ApJL, 238, L129, doi: 10.1086/183272

Sari, R., & Piran, T. 1995, ApJL, 455, L143, doi: 10.1086/309835

Schneider, F. R. N., Ohlmann, S. T., Podsiadlowski, P., et al. 2019, Nature, 574, 211, doi: 10.1038/s41586-019-1621-5

Shakura, N. I., & Sunyaev, R. A. 1973, A&A, 500, 33

Shultz, M., Wade, G. A., Alecian, E., & BinaMIcS Collaboration. 2015, MNRAS, 454, L1, doi: 10.1093/mnrasl/slv096

Sobacchi, E., Lyubarsky, Y., Beloborodov, A. M., & Sironi, L. 2021, MNRAS, 500, 272, doi: 10.1093/mnras/staa3248

Soker, N., & Tylenda, R. 2006, MNRAS, 373, 733, doi: 10.1111/j.1365-2966.2006.11056.x

Soria, R., Hau, G. K. T., Graham, A. W., et al. 2010, MNRAS, 405, 870, doi: 10.1111/j.1365-2966.2010.16517.x

Soria, R., Long, K. S., Blair, W. P., et al. 2014, Science, 343, 1330, doi: 10.1126/science.1248759

Spitler, L. G., Scholz, P., Hessels, J. W. T., et al. 2016, Nature, 531, 202, doi: 10.1038/nature17168

Spruit, H. C., & Uzdensky, D. A. 2005, ApJ, 629, 960, doi: 10.1086/431454

Sridhar, N., Bhattacharyya, S., Chandra, S., & Antia, H. M. 2019, MNRAS, 487, 4221, doi: 10.1093/mnras/stz1476

Sridhar, N., García, J. A., Steiner, J. F., et al. 2020, ApJ, 890, 53, doi: 10.3847/1538-4357/ab64f5

Sridhar, N., Zrake, J., Metzger, B. D., Sironi, L., & Giannios, D. 2021, MNRAS, 501, 3184, doi: 10.1093/mnras/staa3794

Stone, N., & Loeb, A. 2012, PhRvL, 108, 061302, doi: 10.1103/PhysRevLett.108.061302

Sutton, A. D., Roberts, T. P., Gladstone, J. C., et al. 2013a, MNRAS, 434, 1702, doi: 10.1093/mnras/stt1133

Sutton, A. D., Roberts, T. P., & Middleton, M. J. 2013b, MNRAS, 435, 1758, doi: 10.1093/mnras/stt1419

Swartz, D. A., Soria, R., Tennant, A. F., & Yukita, M. 2011, ApJ, 741, 49, doi: 10.1088/0004-637X/741/1/49

Tanaka, Y., & Shibazaki, N. 1996, ARA&A, 34, 607, doi: 10.1146/annurev.astro.34.1.607

Tchekhovskoy, A., McKinney, J. C., & Narayan, R. 2008, MNRAS, 388, 551, doi: 10.1111/j.1365-2966.2008.13425.x

Tchekhovskoy, A., Narayan, R., & McKinney, J. C. 2010, ApJ, 711, 50, doi: 10.1088/0004-637X/711/1/50

—. 2011, Mon. Not. R. Astron. Soc., 418, L79, doi: 10.1111/j.1745-3933.2011.01147.x

Tendulkar, S. P., Bassa, C. G., Cordes, J. M., et al. 2017, ApJL, 834, L7, doi: 10.3847/2041-8213/834/2/L7

Tendulkar, S. P., Gil de Paz, A., Kirichenko, A. Y., et al. 2020, arXiv e-prints, arXiv:2011.03257. https://arxiv.org/abs/2011.03257

Tetarenko, B. E., Sivakoff, G. R., Heinke, C. O., & Gladstone, J. C. 2016, ApJS, 222, 15, doi: 10.3847/0067-0049/222/2/15

The CHIME/FRB Collaboration, :, Andersen, B. C., et al. 2020, arXiv e-prints, arXiv:2005.10324. https://arxiv.org/abs/2005.10324

Thorne, K. S., & Zytkow, A. N. 1975, ApJL, 199, L19, doi: 10.1086/181839

Thornton, D., Stappers, B., Bailes, M., et al. 2013, Science, 341, 53, doi: 10.1126/science.1236789

Tsygankov, S. S., Mushtukov, A. A., Suleimanov, V. F., & Poutanen, J. 2016, MNRAS, 457, 1101, doi: 10.1093/mnras/stw046

Tylenda, R., Hajduk, M., Kamiński, T., et al. 2011, A&A, 528, A114, doi: 10.1051/0004-6361/201016221

Vasilopoulos, G., Lander, S. K., Koliopanos, F., & Bailyn, C. D. 2020, MNRAS, 491, 4949, doi: 10.1093/mnras/stz3298

Vinokurov, A., Fabrika, S., & Atapin, K. 2018, ApJ, 854, 176, doi: 10.3847/1538-4357/aaaa6c

Wadiasingh, Z., Beniamini, P., Timokhin, A., et al. 2020, ApJ, 891, 82, doi: 10.3847/1538-4357/ab6d69

Wadiasingh, Z., & Timokhin, A. 2019, ApJ, 879, 4, doi: 10.3847/1538-4357/ab2240

Walton, D. J., Gladstone, J. C., Roberts, T. P., & Fabian , A. C. 2011, Astronomische Nachrichten, 332, 354, doi: 10.1002/asna.201011498

Walton, D. J., Fürst, F., Bachetti, M., et al. 2016, ApJL, 827, L13, doi: 10.3847/2041-8205/827/1/L13

Wang, Q. D. 2002, MNRAS, 332, 764, doi: 10.1046/j.1365-8711.2002.05317.x

Waxman, E. 2017, ApJ, 842, 34, doi: 10.3847/1538-4357/aa713e

Weng, S.-S., & Feng, H. 2018, ApJ, 853, 115, doi: 10.3847/1538-4357/aaa45c

Wiktorowicz, G., Sobolewska, M., Sadowski, A., & Belczynski, K. 2015, ApJ, 810, 20, doi: 10.1088/0004-637X/810/1/20

Yang, Y.-P., Li, Q.-C., & Zhang, B. 2020, ApJ, 895, 7, doi: 10.3847/1538-4357/ab88ab

Yuan, F., & Narayan, R. 2014, ARA&A, 52, 529, doi: 10.1146/annurev-astro-082812-141003

Yuan, Y., Beloborodov, A. M., Chen, A. Y., & Levin, Y. 2020, ApJL, 900, L21, doi: 10.3847/2041-8213/abafa8

Zanazzi, J. J., & Lai, D. 2020, ApJL, 892, L15, doi: 10.3847/2041-8213/ab7cdd

Zapartas, E., de Mink, S. E., Izzard, R. G., et al. 2017, A&A, 601, A29, doi: 10.1051/0004-6361/201629685

Zhang, B. 2020a, Nature, 587, 45, doi: 10.1038/s41586-020-2828-1

—. 2020b, ApJL, 890, L24, doi: 10.3847/2041-8213/ab7244

Zhong, S.-Q., & Dai, Z.-G. 2020, ApJ, 893, 9, doi: 10.3847/1538-4357/ab7bdf

Zrake, J., & Arons, J. 2017, ApJ, 847, 57, doi: 10.3847/1538-4357/aa826d